

INTEGRATED MEMBRANE PROCESSES FOR AUGMENTING WATER RESOURCES AND SILICA  
RECOVERY AT GEOTHERMAL POWER PLANTS

by  
Emily M. Gustafson

A thesis submitted to the Faculty and the Board of Trustees of the Colorado School of Mines in partial fulfillment of the requirements for the degree of Master of Science (Environmental Engineering Sciences).

Golden, Colorado

Date \_\_\_\_\_

Signed: \_\_\_\_\_

Emily M. Gustafson

Signed: \_\_\_\_\_

Dr. Tzahi Y. Cath

Thesis Advisor

Golden, Colorado

Date \_\_\_\_\_

Signed: \_\_\_\_\_

Dr. John McCray

Professor and Head

Department of Civil and Environmental Engineering

## ABSTRACT

The interdependence of water and energy, or the “water-energy nexus”, exacerbates the stress on both fresh water and energy resources. Power plants require high volumes of water for cooling purposes. Treated impaired groundwater is one alternative source of cooling tower make-up water. These water sources often contain high concentrations of low-solubility minerals such as silica. Oversaturation of silica can cause polymerization, leading to colloidal deposits, which are very difficult to remove from surfaces. Water from a geothermal power plant located in northeastern Nevada was selected for this study. Currently, more than 37% of the make-up water in the plant is wasted as blowdown because of the presence of silica, despite chemical treatment with numerous antiscalants. This study explores the best operating conditions of three membrane treatment processes: nanofiltration (NF), ultrafiltration (UF), and membrane distillation (MD) to enhance water recovery and potentially recover colloidal silica for beneficial use. Dow’s NF90 membrane was selected for testing. A model to predict concentrations of silica on the membrane surface was experimentally validated and used to determine an optimal water recovery of 82% for the treated water. The NF concentrate was used as feed in the UF to concentrate colloidal silica. A sustainable UF operation was achieved, demonstrated through 90% water recovery and 0.4%/w colloidal silica in the concentrate—facilitated by chemically enhanced backwashing. UF was also investigated as pretreatment to NF, clarifying NF concentrate and returning the permeate into the NF feed; however, the operation was unsustainable. Lastly, MD was explored as a desalination process for water recovery from NF concentrate, and demonstrated that 95% water recovery can be achieved when treating water containing high concentrations of silica.

## TABLE OF CONTENTS

ABSTRACT.....	iii
LIST OF FIGURES.....	vi
LIST OF TABLES AND APPENDIX FIGURES.....	viii
LIST OF ABBREVIATIONS.....	ix
LIST OF SYMBOLS.....	x
ACKNOWLEDGMENTS.....	xi
CHAPTER 1 INTRODUCTION.....	1
CHAPTER 2 MATERIALS AND METHODS.....	4
2.1 Solution chemistry and analytical methods .....	4
2.1.1 OLI scaling tendency simulations.....	5
2.1.2 Scanning electron microscopy (SEM) and electron dispersive spectroscopy (EDS) .....	5
2.1.3 Particle analysis.....	5
2.2 Membrane processes.....	5
2.2.1 Nanofiltration.....	6
2.2.1.1 Membranes and modules.....	7
2.2.1.2 Test apparatus.....	7
2.2.1.3 Experimental procedures.....	8
2.2.1.4 Membrane selection tests.....	8
2.2.1.5 Synthetic water experiments.....	8
2.2.1.6 Spiral wound optimization experiments.....	9
2.2.1.7 NF90 scaling experiments.....	12
2.2.2 Membrane distillation.....	13
2.2.2.1 Membranes and spacers.....	13
2.2.2.2 Test apparatus.....	13
2.2.2.3 Experimental procedures.....	15
2.2.3 Ultrafiltration.....	15
2.2.3.1 UF membranes.....	15
2.2.3.2 Test apparatus.....	16
2.2.3.3 Experimental procedures.....	16
2.2.3.4 Permeability tests.....	17
2.2.3.5 Concentration experiments.....	17
CHAPTER 3 RESULTS AND DISCUSSION.....	18
3.1 OLI stream analyzer simulations.....	18
3.2 Nanofiltration.....	18

3.2.1	Membrane selection tests.....	19
3.2.2	Synthetic water experiments.....	20
3.2.3	Optimization of operating conditions.....	21
3.2.4	NF90 scaling experiments.....	22
3.3	Membrane distillation.....	23
3.3.1	MD scaling experiments .....	23
3.3.2	MD concentration experiments.....	25
3.4	Ultrafiltration.....	26
3.4.1	Determination of critical water flux.....	26
3.4.2	Optimization of operating conditions.....	27
3.4.3	UF colloidal silica concentration experiments.....	29
CHAPTER 4	CONCLUSIONS.....	35
	REFERENCES CITED .....	36
	APPENDIX A.....	40

## LIST OF FIGURES

Figure 2-1	A three-step treatment scheme of the MU-S was investigated in this study. Symbols are further described in each sections test apparatus M&M. In flow scheme (1) the MU-S water is treated using NF or RO and the concentrate is collected in a holding tank before being used as feed for the UF. The UF permeate (MU-S <sub>UFP</sub> ) is collected and used as feed again in the NF. In flow scheme (2) the MU-S water is again treated utilizing NF or RO and the concentrate is collected in a holding tank. The concentrate remains in the holding tank for more than 24 hours before it is used as feed in the UF. The UF permeate is then used as the feed stream in MD. The concentrate from the MD is collected in the holding tank.....	6
Figure 2-2	Flow diagram of the NF bench scale apparatus used in the study. Feed was recirculated through a heat exchanger before the cell. Experiments were operated at various flows (2.7–3 LPM) and pressures (3.45 to 20.7 bar (50-300 psi)). A bypass line intermittently returned the permeate stream to the feed tank.....	8
Figure 2-3	MD bench-scale test apparatus. Feed and distillate streams are circulated counter-currently at 1.5 LPM on each side of the membrane. The feed stream is maintained at 60 °C and the distillate stream at 30 °C. A bypass line intermittently returns the distillate to the feed tank to provide a constant feed concentration.....	14
Figure 2-4	Flow schematic of the UF system. Feed was circulated through the modules at a cross-flow velocity of 12-15 cm/s. A peristaltic pump was utilized to provide vacuum pressure and control the flux of permeate. It was also used for backwashing of the membranes.....	16
Figure 3-1	OLI prediction of dominant scaling tendencies for (a) SiO <sub>2</sub> and (b) CaCO <sub>3</sub> , of T-MU based on water recovery (0 to 90%) and temperature (10 to 70 °C).....	18
Figure 3-2	(a) Water flux, (b) % salt rejection, and (c) % silica rejection (c) were compared for three NF and one RO membranes (NF DK, NF 245, NF90, and RO SE). 5-hour experiments were performed using flat sheet modules (0.0139 m <sup>2</sup> ) for three feed waters: MU-T at 20 °C, 2,000 mg/L NaCl at 20 °C, and BI-T at 70 °C. Feed batches were circulated through the test cell at 1 LPM. Experiments were conducted at constant pressure of 10.3 bar (150 psi) for the MU-T and BI-T waters and 20.7 bar (300 psi) for the NaCl feed waters.....	19
Figure 3-3	(a) Water flux as a function of feed pressure and (b) percent ion rejection during experiments comparing MU-S to the MU-T water. Experiments were conducted with the NF90 membrane. Water was circulated at 1 LPM and was kept at 20±1 °C. Data for ion rejection is from experiments conducted at 10.3 bar.....	21
Figure 3-4	(a) Measured concentrations (circle) of silica as a function of % water recovery compared to modeled concentrations in the bulk (diamond) and at the membrane surface (square) as predicted by equations 1 to 21; and (b) predicted concentrate flow and corresponding % water recovery assuming a water flux of 50 LMH as a function of the number of membrane modules connected in series and a maximum concentration of 600 mg/L SiO <sub>2</sub> on the membrane surface. Experiments were conducted utilizing one to four NF90-2540 spiral wound modules (2.6-10.4 m <sup>2</sup> ). MU-S feed was circulated at 3 LPM and constant pressure was maintained at 20.7 bar.....	22
Figure 3-5	Water flux as a function of time for the NF90 flat sheet membranes (139 cm <sup>2</sup> ) utilizing the 8x MU-S (squares) and 8x MU-S <sub>UFP</sub> (triangles) as feed waters. Feed water	

	was circulated at 1 LPM and experiments were operated at 10.3 bar.....	23
Figure 3-6	Water flux as a function of time utilizing (a) 3M PP 0.2 $\mu\text{m}$ (b) Clarcor QL822 (c) Aquastill 0.3 micron membranes. Feed and distillate streams were circulated through the MD modules (194 $\text{cm}^2$ ) at 1.5 LPM utilizing 8x MU-S and 8x MU-S <sub>UFP</sub> at 30/60 $^{\circ}\text{C}$ . An additional experiment with the 3M membrane and 8x MU-S was performed utilizing a cartridge filter in the feed line.....	24
Figure 3-7	Experiments were performed utilizing one 3M membrane and 6x MU-S <sub>UFP</sub> as the feed stream. Four batches of increasing volume (5-8 L) were circulated through the module (0.0194 $\text{m}^2$ ) at 1.5 LPM and a temperature difference of 30/60 $^{\circ}\text{C}$ .....	25
Figure 3-8	MD concentrate of 8x MU-S <sub>UFP</sub> at pH 8 and adjusted to pH 9-12 (left) (b) Concentrations of ions in the supernatant and the floc of the MD concentrate 8x MU-S <sub>UFP</sub> after 87% recovery.....	26
Figure 3-9	(a) Water flux as a function of TMP and (b) water flux and TMP as a function of time. Feed water was circulated at 1 LPM, corresponding to cross flow velocity of 15 $\text{cm/s}$ , for 10 minutes at each water flux from 5 to $\sim 50$ LMH utilizing a 0.0125 $\text{m}^2$ UF membrane module. Permeability of pure water (diamond) and 8x MU-S (circles) as feed.....	27
Figure 3-10	(a) permeability tests performed before the experiment, after 90% recovery, and after CEB during the first test, (b) TMP as a function of time up to 90% water recovery with automatic backwashing every 30 minutes as demonstrated by the fluctuations during the first test, (c) permeability tests performed before the experiment, after 90% recovery, and after CEB during the second test, and (d) TMP as a function of time up to 90% water recovery with automatic backwashing triggered by an increase in TMP during the second test. Backwash is seen by the drop in TMP to 0. ....	28
Figure 3-11	Water flux as a function of TMP during UF testing with 144 liters of NF concentrate at 6x MU-S. Permeability tests with deionized water feed were conducted before the experiment, after 85 and 90% water recovery of 144 L was achieved, and after each CEB utilizing 5 L of a pH 12 NaOH solution. Feed was circulated at 15 $\text{cm/s}$ cross-flow velocity at a constant temperature of $20\pm 1$ $^{\circ}\text{C}$ . The permeability of each 250 $\text{cm}^2$ module was tested separately but both had similar results.....	29
Figure 3-12	Feed water after 95% water recovery before separating floc and supernatant (left) and separated floc (right).....	30
Figure 3-13	Total and colloidal silica concentrations as a function of water recovery. Concentrations were compared to the predicted values utilizing mass balance and equations 1, 2, and 5 and the initial measured feed concentrations of total and colloidal silica.....	31
Figure 3-14	(a) SEM micrograph at 100x magnification and (b) EDS chromatograph of a silica gel recovered from the UF membrane modules after 95% recovery. The gel was freeze dried for 24 hours before analysis.....	32
Figure 3-15	Particle size analysis of silica in 6x MU-S, after 75% water recovery, and after 95% water recovery (supernatant and floc) for the UF concentration experiments.....	33
Figure 3-16	(a) % composition of all ions in the UF feed water after 75% and 90% water recovery. (b) UF rejection of all ions in the feed water after 90% water recovery.....	34

## LIST OF TABLES AND APPENDIX FIGURES

Table 2-1	Water quality of the make-up water and cooling tower brine injection water for the field samples (MU-T; BI-T) and the synthetically matched water (MU-S, BI-S). Concentrations are measured in mg/L and alkalinity is measured in mg/L as CaCO <sub>3</sub> .....	4
Table 2-2	Characteristics of membrane distillation membranes provided by the manufacturers.....	13
Table 3-1	Water quality of the 8x MU-S UF feed water after 0%, 75%, 90%, and 95% water recovery, measured using IC and ICP methods. 95% water recovery was separated into two samples based on composition: supernatant 95% (S) and flocc 95% (F). Concentrations were measured in mg/L.....	33
Figure A-1	Integrity of each membrane before and after model validation experiments. Integrity tests were operated at 3 LPM, 20.7 bar and 20 °C utilizing a 2,000 mg/L NaCl solution.....	40
Figure A-2	The permeability of UF membrane (0.025 m <sup>2</sup> ) utilizing pure water and 8x MU-S. Feed water was circulated at 2 LPM, corresponding cross flow velocity of 30 cm/s, for 10 minutes at each water flux from 5-50 LMH.....	40
Figure A-3	TMP based on water recovery and time utilizing 144 L of 6x MU-S. The experiment was performed utilizing two (0.0250 m <sup>2</sup> ) modules in parallel. Feed was circulated at 2 LPM corresponding to 15 cm/s cross-flow velocity of each module. CEB backwashing was performed after 85% water recovery and after 90% water recovery demonstrated by the drop in TMP.....	41
Figure A-4	Measured and predicted concentrations of silica in the MD feed. Experiments were performed utilizing one 3M membrane and 6x MU-S <sub>UFP</sub> as the feed stream. Four batches of increasing volume (5-8 L) were circulated through the module (0.0194 m <sup>2</sup> ) at 1.5 LPM and a temperature difference of 30/60 °C.....	41

## LIST OF ABBREVIATIONS

BI	Brine injection
DCMD	Direct contact membrane distillation
ESEM	Environmental scanning electron microscope
EDS	Electron dispersive spectroscopy
LMH	Liters per meter squared per hour
LPM	Liter per minute
ePTFE	Polytetrafluoroethylene
PVC	Polyvinyl chloride
MU	Make-up water
MD	Membrane distillation
NF	Nanofiltration
O&M	Operation and maintenance
PP	Polypropylene
RO	Reverse osmosis
SWRO	Seawater reverse osmosis
TDS	Total dissolved solids
TMP	Transmembrane pressure
TEM	Transmission electron microscopy
UF	Ultrafiltration
ZLD	zero-liquid discharge

## LIST OF SYMBOLS

$A_m$	Membrane area
$c_b$	Bulk concentration of SiO <sub>2</sub> in the concentrate
$c_f$	Feed concentration
$c_p$	Permeate concentration
$c_m$	Concentration of SiO <sub>2</sub> at the membrane surface
$D$	Diffusion coefficient of the solute
$d_f$	Diameter of spacer filament
$d_h$	Hydraulic diameter
$h_{sp}$	Spacer thickness
$J_w$	Flux of water across the membrane
$k$	Mass transfer coefficient from the film layer model
$k_{dc}$	Sherwood spacer correction factor
$L$	Feed channel length
$l_m$	Mesh size
$Q_c$	Concentrate flow
$Q_f$	Feed flow
$Q_p$	Permeate flow
$r$	Recovery
$Re$	Reynolds number
$R_m$	Rejection on the membrane
$R_{mod}$	Measurable rejection of the membrane in the module
$Sc$	Schmidt number
$Sh$	Sherwood number
$s_{sp}$	Spacer surface
$S_{vsp}$	Specific surface of the spacer.
$u$	Cross-flow velocity on the exit of the module
$V_{sp}$	Spacer volume
$w$	Width of the channel
$\epsilon$	Spacer voidage
$\theta$	Angle spacer
$\mu$	Viscosity
$\rho$	Density

## ACKNOWLEDGEMENTS

I would like to express my sincere appreciation to my committee and all those who assisted in my research, without their guidance and encouragement this work would not have been possible. Thank you for making me the engineer I am today.

First and foremost, I would like to thank my advisor Dr. Tzahi Cath for his constant support and for always challenging me to be a better researcher and writer. I sincerely appreciate the chance you took by asking me to be a part of this project and offering me an opportunity I could not refuse. I owe a debt of gratitude to my committee member Dr. Johan Vanneste, who was a mentor to me on this project. I would have been lost without his enthusiasm, continuous direction, and his ability to always break the tension (usually with food or weird words). I am also deeply grateful to Mike Veres, Tani Cath, Kate Spangler, Estefani Bustos, Craig Turchi, and my committee member Dr. Christopher Bellona, for all of their research assistance and instruction throughout the project.

I am extremely grateful for the financial support from the Department of Energy for this project and to the Edna Bailey Sussman Foundation and the National Renewable Energy Laboratory for giving me the opportunity to continue my research during a summer internship. I would also like to thank WateReuse Colorado for their 2017 Student Scholarship and Koch Industries, Dow Filmtec, G.E., 3M, CLARCOR, and Aquastill for providing membranes for this study.

Last, but not least, I would like to thank my family and friends for their endless encouragement and for consistently reminding me to always be optimistic. I am forever grateful for the unconditional love that I received from my mom, Eleanor Gustafson, my sister, Maggie Gustafson, and my partner, Andreas Apostol.

## CHAPTER 1 INTRODUCTION

In the western United States, where drought is most prevalent, water scarcity is exacerbated by the increasing demand for clean water. Therefore, developing technologies for the treatment of unconventional sources such as impaired groundwater is critical. Currently, the reuse of reclaimed water from municipal and various industrial sources is already being investigated and implemented [1-4]. Membrane desalination technologies are of particular interest because they have demonstrated the ability to treat challenging waste streams [5, 6]. However, despite technological advancements, desalination processes still utilize more energy than conventional water treatment [7]. Desalination processes consume 75.2 TWh of energy per year worldwide, with seawater reverse osmosis (SWRO) consuming approximately 3 to 4 kWh/m<sup>3</sup> [7, 8]. Meanwhile, as the demand for energy continues to increase, the stress on freshwater resources intensifies. This is also known as the energy-water nexus or “the relationship between how much water is consumed to generate and transmit energy, and how much energy it takes to collect, clean, move, store, and dispose of water” [7, 9].

Renewable energy can be an emerging alternative source of energy to support desalination, and the abundance of geothermal resources across the western U.S. can help offset the strain on other energy sources such as coal, oil, and gas. Geothermal energy offers a surplus of low-temperature heat that is otherwise underutilized because it is unsuitable for power production [10]. Developing desalination technologies capable of utilizing the low-grade heat while producing high quality water could lower operation and maintenance (O&M) costs and reduce the stress on depleting water sources. Although not often considered, 40% of freshwater withdrawals in the western US is used for power plants, which require large volume of water for cooling purposes [11]. Cooling towers lose large volumes of water to evaporation and also produce wastewater in the form of cooling tower blowdown [12].

While the sources of fresh clean water are rapidly declining, treated impaired groundwater and cooling tower blowdown are desired as alternative sources of cooling make-up water. These water sources often contain high concentrations of total dissolved solids (TDS), including calcium, magnesium, and silica, that have high scaling potential [13-15]. Scaling due to silica is a particularly challenging problem because when silica is concentrated beyond its saturation point, it has the potential to form a hard scale that is difficult to remove.

Silicon (Si) is the second most abundant element on earth after oxygen. It is present in most rocks as the mineral quartz, which is composed of the naturally occurring crystalline compound silicon dioxide, SiO<sub>2</sub>, or more commonly known as silica. Silica is found in most natural water sources due to the dissolution of rock into the groundwater. The hard scale formed by silica is the result of a complex chemistry that occurs when SiO<sub>2</sub> is dissolved in water [16]. At low concentrations, it exists as a simple silicate in ionic form (SiO<sub>4</sub><sup>4-</sup>); however, the solubility of silica in water is low with a limit of approximately

120 mg/L [16]. Once silica has passed the point of saturation, it begins to polymerize and to form amorphous colloidal silica [17]. The saturation point of silica and the succeeding induction time of colloid formation depends on many factors, including temperature, pH, concentration, and interactions with other ions present in solution [16]. The solubility of silica increases significantly at higher temperatures and above pH of 9 [16]. Both low and high pH reduce the rates of polymerization, with the highest rates of polymerization occurring at pH of 7.5 [18]. The induction time before polymerization occurs also decreases as the concentration of silica increases [19].

The formation and deposition of colloidal silica is common in desalination processes because of the natural pH of most waters [13], concentration of the ions due to high rejection, and the concentration polarization occurring at the membrane surface [20]. Pressure-driven membrane processes such as reverse osmosis (RO) and nanofiltration (NF) have been proven to remove colloidal silica, but at the expense of reducing water flux due to scaling [21]. Once silica scaling occurs, these membranes become more resistant to simple cleaning methods such as acid washing or commercial cleaners [22]. Pretreatment through coagulation or the use of antiscalants are both viable, but costly and inefficient. Antiscalants become less effective at higher silica concentrations [15] while coagulation incompletely removes silica and produces large amounts of sludge [18, 21, 22]. Therefore, mitigation of colloidal silica is necessary and can be achieved by manipulating the operating conditions of desalination.

pH adjustment techniques could be beneficial for preventing silica scaling; however, softening pretreatment would be necessary to prevent other scaling tendencies that occur at high pH, such as calcium carbonate ( $\text{CaCO}_3$ ) [23]. High concentrations of dissolved solids also cause an increase in osmotic pressure; therefore, limiting water recovery in pressure-driven processes such as RO and NF [13, 24]. Operating NF or RO processes at higher temperatures would be a second strategy for silica scaling mitigation; however, most high-pressure membranes are rated for maximum operating temperatures of 40 °C [25]. The third method for mitigating the formation of colloidal silica would be to impede silica polymerization by operating the membrane processes at a lower recovery and limit the concentrations of silica in the concentrate stream; however, for land-locked states that cannot discharge concentrated brine into the ocean, this presents the challenge of finding an affordable environmental means for disposal of the concentrate brine. Land application is one option for disposal; however, studies have shown that this could negatively impact the soil and the groundwater [26].

One alternative strategy for reducing the environmental impacts of desalination is to employ a zero-liquid discharge (ZLD) operation. Higher water recovery can be achieved by collecting the concentrate from NF or RO and utilizing other desalination processes that are not limited by osmotic pressure and can withstand higher temperatures to increase solubility. One emerging technology is desalination through membrane distillation (MD). MD uses partial vapor-pressure differences across a hydrophobic, microporous membrane to promote water evaporation through the pores and produce high quality water [18]. Unlike its high-pressure-driven competitor, RO, MD operates at near-ambient pressure and can treat higher salinity brines. [27-33]. Although it has been shown to have higher overall energy consumption,

MD relies primarily on low-grade heat. Utilizing the surplus of low temperature geothermal heat can offset the economic costs, putting MD at an advantage.

Another approach for reducing the waste streams from desalination processes is to recover minerals from their brines [34]. The commercial recovery of minerals such as potassium and magnesium salts has already been demonstrated utilizing hypersaline brines from the Great Salt Lake and the Dead Sea [35, 36]. Mineral extraction from some geothermal brines has also been explored [37-39]. Because of the abundance and its unique chemical properties, silica has numerous historical uses, including manufacturing glass, paper, ceramics, and silicones [40]. It is also utilized for concrete and other materials used for construction of buildings and roadways [41]. Therefore, recovering colloidal silica from the geothermal waters could possibly offset the costs of desalination [34]. One method for recovering colloidal silica is to filter high concentration waters using ultrafiltration (UF) [42]. UF is a low-pressure process that utilizes porous membranes to remove nano-scale particles and colloids from water; commonly removing bacteria, viruses, turbidity, and larger particles from source water in municipal and industrial water and wastewater treatment plants [43]. Due to the large pore size, most monovalent and divalent ions, such as sodium, chloride, calcium, and magnesium, pass through the UF membrane [44]. Separating salts from silica solutions will increase the purity and result in a higher market value [34].

The main objective of this study was to investigate the treatment of impaired geothermal waters containing high concentrations of silica by a three-step treatment scheme consisting of NF, UF, and MD. Experiments were performed to optimize water recovery and mitigate membrane scaling for sustainable membrane treatment. Another goal of this study was to demonstrate the ability of UF to recover pure colloidal silica from the NF brine. Membrane performance was assessed by monitoring the rejection of inorganic constituents and the occurrence of membrane scaling, exhibited by water flux decline and increases in transmembrane pressure (TMP).

CHAPTER 2  
MATERIALS AND METHODS

This chapter discusses the design and operating conditions of three membrane processes in a treatment scheme. Please note that in this section we bundle together the presentation of membrane selection, test apparatus, and experimental procedures for each membrane process tested.

**2.1 Solution chemistry and analytical methods**

Two types of geothermal waters were used in this study, cooling towers make-up water (MU) and cooling towers brine injection water (BI). Both waters were collected from an Ormat Technologies geothermal power plant in Tuscarora, Nevada. The samples were shipped overnight to Golden, CO. Ion chromatography (IC; ICS-90, Dionex, Sunnyvale, CA) and inductively coupled plasma – atomic emission spectroscopy (ICP-AES; Optima 5300, Perkin-Elmer, Fremont, CA) analyses were conducted on both samples to determine the concentration of major anions and cations, respectively [45]. ICP-AES samples were acidified with nitric acid to a pH of 2.

The sampled waters were then synthetically reproduced (MU-S; BI-S) to match all the constituents and their concentrations to those in the Tuscarora samples (MU-T; BI-T) (Table 2-1). Due to chemical balancing, the only constituents that were substantially different in concentration were sodium and chloride. The synthetic solutions were prepared by initially adding  $\text{Na}_2\text{SiO}_3 \cdot 5\text{H}_2\text{O}$  to deionized water.  $\text{Na}_2\text{SiO}_3 \cdot 5\text{H}_2\text{O}$  is a base and raises the pH to above 12 for 90 and 220 mg/L solutions. The pH of the solution was then adjusted to approximately 7 using concentrated HCl before adding the other chemicals. Experiments were conducted to compare the performance of the membranes using the field samples and the synthetic solutions. UF and MD experiments were conducted utilizing the synthetic solution at least 24 hours after it was prepared.

Soluble silica concentrations were measured using Silica method 8185 for high range samples (1 to 100 mg/L) and Silica method 8186 for low-range samples (0.010 to 1.6 mg/L) on a HACH DR 5000 spectrophotometer [46]. Total silica and other constituents were measured using IC and ICP methods listed above. Colloidal silica concentrations were then calculated by subtracting soluble silica concentrations from total silica.

Table 2-1. Water quality of the make-up water and cooling tower brine injection water for the field samples (MU-T; BI-T) and the synthetically matched water (MU-S, BI-S). Concentrations are measured in mg/L and alkalinity is measured in mg/L as  $\text{CaCO}_3$ .

	$\text{Na}^+$	$\text{K}^+$	$\text{Mg}^{2+}$	$\text{Ca}^{2+}$	$\text{Ba}^{2+}$	$\text{Cl}^-$	$\text{SO}_4^{2-}$	$\text{SiO}_2$	Alkalinity	pH
<b>MU-T</b>	23.5	8.94	2.45	9.59	0.220	8.33	12.4	90	84	7.0
<b>MU-S</b>	111	10.1	2.75	10.1	0.261	206	17.3	87	85	7.1
<b>BI-T</b>	128	15.4	0.036	3.03	0.126	19.9	50.1	220	260	7.0
<b>BI-S</b>	278	16.6	0.198	3.08	0.116	130.4	57.4	240	262	7.2

Currently the geothermal treatment plant recycles the MU-T water in the cooling tower. Calculated from the flows of the make-up water supply and the cooling water blowdown, more than 37% of the MU-T is lost as blowdown. This corresponds to about 2.7 cycles of the MU-T in the cooling tower before being injected back into the cool water well. Increasing the number of cycles will substantially decrease the amount of water that is withdrawn for cooling water and therefore decrease operation and maintenance costs.

### **2.1.1 OLI scaling tendency simulations**

OLI Stream Analyzer (OLI systems Inc., Cedar Knolls, NJ) was used to estimate the scaling tendency of the T-MU as a function of water recovery and temperature. Stream Analyzer calculates scaling tendency using the saturation ratio (or the ratio of the solution solubility product to the thermodynamic limit based on the thermodynamic equilibrium constant) [47].

### **2.1.2 Scanning electron microscopy (SEM) and electron dispersive spectroscopy (EDS)**

A gel found on the UF membranes after 95% water recovery was collected for analysis. The sample was freeze-dried for 24 hours to preserve structural features of the precipitate (Pecoraro, 1995) using a FreeZone 6 (Labconco, Kansas City, MO) at -50 °C and under constant pressure of 0.12 millibar (mbar). Micrographs were generated with environmental scanning electron microscope (ESEM) (Hitachi TM-1000 microscope, Tokyo, Japan). Electron dispersive spectroscopy (EDS) was performed on the micrographs utilizing an XFlash 430H EDS detector (Bruker Corporation, Billerica, MA) connected to a computer with QUANTAX 50 microanalysis software. Micrographs were taken at 100x magnification (~1 mm).

### **2.1.3 Particle analysis**

Samples collected from the UF feed after 75 and 95% recovery were shipped to Pall Corporation (Port Washington, NY) for particle analysis. Particle size measurements were performed utilizing a particle sizing systems AccuSizer instrument (Model FX, Santa Barbara, CA). Injection volume was 5 mL.

## **2.2 Membrane processes**

Some of the membrane processes that were tested in this study were utilized in different ways. For example, UF was tested as pretreatment for NF concentrate before returning to the NF feed. It was also tested as a pretreatment for NF concentrate before desalination with MD, and for recovering colloidal silica formed in the NF concentrate or MD concentrate. NF was used for high-recovery desalination of makeup water and in an attempt to increase the recovery by treating the concentrate after UF pretreatment. The performance of the NF membrane using pretreated NF concentrate as feed was compared to the performance of MD also using the pretreated NF concentrate. Therefore, there were two possible treatment schemes as illustrated in Figure 2-1.

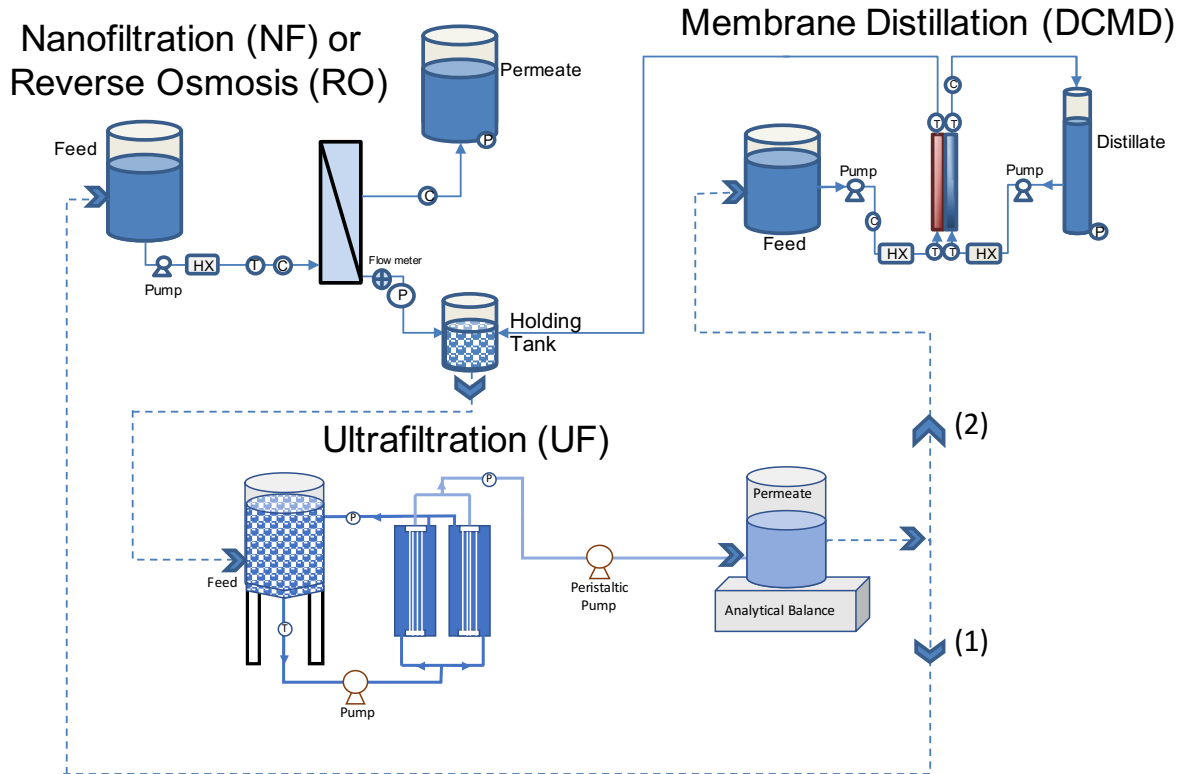


Figure 2-1. A three-step treatment scheme of the MU-S was investigated in this study. Symbols are further described in each sections test apparatus M&M. In flow scheme (1) the MU-S water is treated using NF or RO and the concentrate is collected in a holding tank before being used as feed for the UF. The UF permeate (MU-S<sub>UFP</sub>) is collected and used as feed again in the NF. In flow scheme (2) the MU-S water is again treated utilizing NF or RO and the concentrate is collected in a holding tank. The concentrate remains in the holding tank for more than 24 hours before it is used as feed in the UF. The UF permeate is then used as the feed stream in MD. The concentrate from the MD is collected in the holding tank.

In scheme (1) MU-S water is treated utilizing NF or RO. The concentrate is collected in a holding tank then used as feed for the UF. The permeate from the UF is collected and used as feed in the NF or RO to increase total water recovery and initiating a second cycle between NF and UF. For scheme 2 the first two steps are the same as in scheme 1; however, in scheme (2) the permeate from the UF is collected and used as feed for the MD process. The MD concentrate is then collected and used as feed for the UF, again initiating cycles between UF and MD. The performance of the NF membrane was compared to the MD membranes.

### 2.2.1 Nanofiltration

NF was the first process utilized in the treatment scheme for high water recovery desalination. NF experiments were performed using MU-S as the feed. Two membrane modules were tested utilizing flat-sheet and spiral wound membranes. Experiments were also performed to investigate the scaling tendency of the NF concentrate and the performance of the NF90 membrane utilizing pretreated NF concentrate.

### **2.2.1.1 Membranes and modules**

Three flat sheet NF membranes and one flat sheet RO membrane were tested to select the best membrane for further testing, using water flux and solute rejection as performance criteria when treating the MU-S and BI-S waters. Two NF membranes were obtained from Dow Filmtec (NF245 and NF90, Midland, MI), while the third NF membrane and the RO membrane were acquired from General Electric (GE) (NF DK series and RO SE series, Boston, MA). A stainless steel, SEPA-CF test cell (GE Water & Process Technologies, Trevose, PA) with an active membrane surface area of 139 cm<sup>2</sup>, was used to test the flat sheet membranes. A tricot warp knit (Hornwood Inc., Lilesville, NC) spacer, with 20 carrier channels per inch, was installed in the permeate channel of the flow cell, while an extruded mesh spacer was installed in the feed channel. For each set of experiments, a new membrane coupon was cut and installed in the SEPA-CF flow cell. The NF90 membrane was selected for further testing utilizing both the SEPA-CF flow cell and spiral-wound modules acquired from Dow Filmtec (NF90-2540) with a total membrane area of 2.6 m<sup>2</sup> each.

### **2.2.1.2 Test apparatus**

A flow schematic of the bench-scale apparatus is illustrated in Figure 2-2. The experimental setup was used for testing of both the flat sheet membranes (SEPA-CF) and the spiral wound membranes. A 30 L stainless steel-304 feed tank was used for experiments with the flat sheet experiments and a 757 L conical-bottom feed tank was used for experiments with the spiral wound membrane module. The tanks were connected to a high-pressure diaphragm pump (Hydra-cell Model No. D10E, Wanner Engineering Inc., Minneapolis, MN) that circulated the feed through a heat exchanger before entering the membrane module. Permeate was collected in a 14 L polyvinyl chloride (PVC) tank that was fitted with a solenoid valve to intermittently return the permeate stream to the feed tank to maintain constant feed concentration. The permeate tank was also fitted with a pressure transducer (PX309 series, OMEGA Engineering, Stamford, CT) at the bottom to measure the hydrostatic pressure of the water and thus the depth and volume of water in the tank.

A SCADA system (LabVIEW, National Instruments, Austin, TX; and UE9/U3, LabJack Corporation, Lakewood, CO) was used to record the water level in the permeate tank and calculate the water flux based on changes in levels in the tank. The SCADA system was also used to control operating conditions, including feed flow, feed temperature, and feed pressure. Conductivity was measured using a toroidal conductivity sensor (Sensorex, Garden Cove, CA) installed in the feed line and a conductivity probe (alpha COND500, Eutech Instruments, Vernon Hills, IL) in the permeate line—both were utilized to automatically calculate salt rejection. A proportional valve (Hass Manufacturing Co., Averill Park, NY) was used to control the feed pressure and a pressure transducer (Omega Engineering, Stamford, CT) was installed before the valve to monitor and facilitate control of the feed pressure. A proportional valve was also used to control the flow of processed chilled water into the heat exchanger to maintain constant temperature, which was monitored using a resistance thermal detector (Model EI1034, LabJack

Corporation, Lakewood, CO). For spiral wound experiments, the flow scheme was slightly modified to operate in an open loop mode (Figure 2-1). Instead of returning the concentrate to the feed, the concentrate was collected in a 200 L drum.

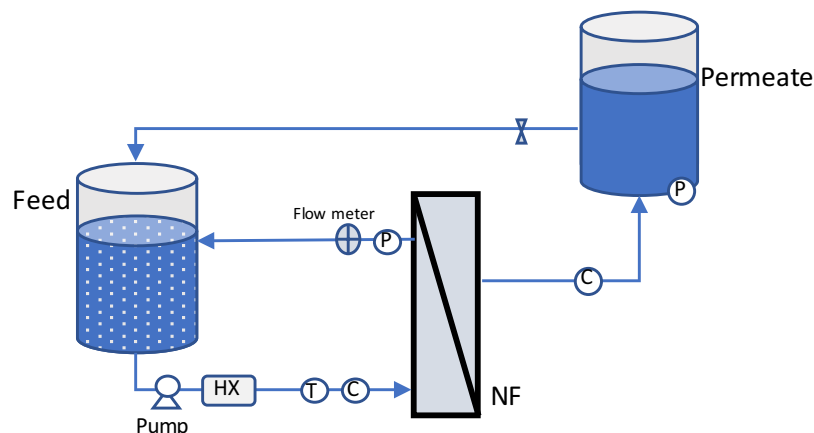


Figure 2-2. Flow diagram of the NF bench scale apparatus used in the study. Feed was recirculated through a heat exchanger before the cell. Experiments were operated at various flows (0.5–3 LPM) and pressures (3.45 to 20.7 bar (50-300 psi)). A bypass line intermittently returned the permeate stream to the feed tank. P- pressure gauge, C- conductivity gauge, T- temperature sensor, HX- heat exchanger.

### 2.2.1.3 Experimental procedures

Initial experiments were conducted to select a membrane for further testing of the make-up water. Experiments with spiral-wound membranes were used to investigate the best operating conditions to optimize water recovery while mitigating silica scaling.

### 2.2.1.4 Membrane selection tests

Membrane selection experiments were conducted at the bench-scale to evaluate rejection and water flux of the NF DK, NF 245, NF90, and RO membranes utilizing three waters: MU-T at  $20 \pm 1$  °C, BI-T at  $70 \pm 1$  °C, and a baseline water of 2,000 mg/L NaCl at  $20 \pm 1$  °C. Feed batches of 5 L were recirculated through the system at 1 L/min (LPM) under constant pressure (10.3 bar (150 psi) for the MU-T and BI-T waters and 20.7 bar (300 psi) for the baseline solution).

### 2.2.1.5 Synthetic water experiments

After the NF90 membrane was selected, an experiment was conducted to evaluate the effect of utilizing synthetically reproduced water compared to the field sample. A 5 L batch of each water was circulated through the system under constant pressure at increments of 3.45 bar (50 psi) from 3.45 to 20.7 bar (50-300 psi). Water flux was monitored and recorded. Samples of the feed and permeate were collected and analyzed using the IC and ICP to calculate rejection of all ions present in the water.

### 2.2.1.6 Spiral wound optimization experiments

Experiments with the NF90-2540 membrane were conducted to optimize operating conditions to minimize/eliminate silica scaling. All membranes were pre-compacted for 20 hours before conducting experiments to distinguish water flux decline due to scaling from compaction. A 2,000 mg/L NaCl feed solution was used for compaction and circulated at 3 LPM under constant pressure of 20.7 bar (300 psi), and the temperature of the feed was maintained at  $20 \pm 1$  °C. After compaction, a baseline rejection test was performed to evaluate membrane integrity using the same operating conditions as during compaction. After every experiment, membrane integrity was tested. If water flux or rejection declined by more than 10% from the baseline rejection test, a pH 11 NaOH solution was circulated through the module for 12 hours to clean the membrane.

The concentration of silica at the membrane surface due to concentration polarization was predicted for different operating conditions. Input variables included membrane area ( $A_m$ ), permeate flow ( $Q_p$ ), concentrate flow ( $Q_c$ ), feed concentration ( $c_f$ ), permeate concentration ( $c_p$ ), and feed channel length ( $L$ ). All operating conditions were optimized to reach the highest water recovery without exceeding a concentration of 720 mg/L  $\text{SiO}_2$ , or the point of zero induction time, on the membrane surface [19]. A modeling approach was adopted to calculate the rejection of solutes on the membrane surface and compare it to the directly measurable rejection of the membrane [48]. The model was utilized to optimize the maximum flow of concentrate based on a membrane surface concentration of 600 mg/L  $\text{SiO}_2$ . 600 mg/L  $\text{SiO}_2$  was selected instead of 720 mg/L in order to protect the membrane, because the concentration at the membrane surface cannot be measured directly. To validate the model, the bulk concentration of  $\text{SiO}_2$  in the concentrate ( $c_b$ ) was measured and compared to the model-predicted value under different operating conditions:

$$c_b = c_f(1 - r)^{-R_{mod}} \quad (1)$$

where  $r$  is water recovery and  $R_{mod}$  is the measurable rejection of the membrane in the module:

$$R_{mod} = \frac{c_f - c_p}{c_f} = 1 - \frac{c_p}{c_f} \quad (2)$$

Water recovery, or the fraction of permeate that is recovered from the feed, was calculated utilizing the mass balance of flow:

$$Q_f = Q_p + Q_c \quad (3)$$

and

$$r = \frac{Q_p}{Q_f} \quad (4)$$

therefore,

$$r = \frac{Q_p}{Q_p + Q_c} \quad (5)$$

where  $Q_f$  is the feed flow.  $Q_p$  was measured and controlled by three independent variables,  $Q_c$ , pressure,  $A_m$ , that were adjusted to achieve target operating conditions.  $Q_p$  could also be utilized with membrane area,  $A_m$ , to calculate the flux of water ( $J_w$ ) across the membrane:

$$J_w = \frac{Q_p}{A_m} \quad (6)$$

With  $R_{mod}$  and  $r$  defined, the rejection of the membrane ( $R_m$ ) could be derived from the equation for  $c_p$  as defined by Mulder [48]:

$$\frac{c_p}{c_f} = \frac{1}{r} [1 - (1 - r)^{1 - R_m}] \quad (7)$$

by utilizing Equation 2 and setting it equal to equation 7:

$$1 - R_{mod} = \frac{1}{r} [1 - (1 - r)^{1 - R_m}] \quad (8)$$

and solving for  $R_m$ :

$$r(1 - R_{mod}) = 1 - (1 - r)^{(1 - R_m)}$$

$$1 - r(1 - R_{mod}) = (1 - r)^{(1 - R_m)}$$

$$\frac{\ln[1 - r(1 - R_{mod})]}{\ln(1 - r)} = (1 - R_m)$$

$$R_m = 1 - \frac{\ln[1 - r(1 - R_{mod})]}{\ln(1 - r)} \quad (9)$$

Utilizing the predicted rejection occurring at the membrane surface, the concentration of  $\text{SiO}_2$  at the membrane surface ( $c_m$ ) could also be calculated [48]:

$$c_m = c_b \left[ \frac{\exp\left(\frac{J_w}{k}\right)}{R_m + (1 - R_m) \exp\left(\frac{J_w}{k}\right)} \right] \quad (10)$$

where  $k$  is the mass transfer coefficient from the film layer model [49]. Variables controlled by fluid dynamics are necessary to understand the nature of the flow and define the mass transfer coefficient

including the Schmidt number ( $Sc$ ; the ratio of kinematic viscosity and mass diffusivity), the Reynolds number ( $Re$ ; ratio of inertial forces to viscous forces, a parameter describing laminar or turbulent flow conditions), and the Sherwood number ( $Sh$ ; the ratio of convective mass transfer to the rate of diffusive mass transports). The Sherwood number is utilized to calculate the mass transfer coefficient [49]:

$$k = \frac{S_h D}{d_h} \quad (11)$$

where  $D$  is the diffusion coefficient of the solute. For silica, Applin et al. experimentally measured the diffusion coefficient of  $\text{Si(OH)}_4$  and found it to be  $2.2 \times 10^{-9} \text{ m}^2 \text{ s}^{-1}$  [50]. The hydraulic diameter ( $d_h$ ) is defined as [49]:

$$d_h = \frac{4\epsilon}{(2/h_{sp}) + (1-\epsilon)S_{vsp}} \quad (12)$$

where  $h_{sp}$  is the spacer thickness,  $\epsilon$  is the spacer voidage:

$$\epsilon = 1 - \frac{\pi d_f^2}{2l_m h_{sp} \sin \theta} \quad (13)$$

and  $S_{vsp}$  is the specific surface of the spacer. The specific surface of the spacer is defined as:

$$S_{vsp} = \frac{S_{sp}}{V_{sp}} \quad (14)$$

where  $V_{sp}$  is the spacer volume:

$$\begin{aligned} V_{sp} &= \frac{1}{2} \left\{ \frac{2\pi d_{f1}^2 l_{m2}}{4} + \frac{2\pi d_{f2}^2 l_{m1}}{4} \right\} \\ &= \frac{\pi}{4} (d_{f1}^2 l_{m2} + d_{f2}^2 l_{m1}) \end{aligned} \quad (15)$$

and  $S_{sp}$  is the spacer surface:

$$S_{sp} = \frac{1}{2} \{ 2\pi d_{f1} l_{m2} + 2\pi d_{f2} l_{m1} \} \quad (16)$$

Data on the spacer was not provided, so it was assumed to be symmetrical and have similar characteristics to Conwed (Minneapolis, MN) 28 Mills RO feed spacer including spacer thickness ( $h_{sp}$ ), diameter of spacer filament ( $d_f$ ), mesh size ( $l_m$ ), and an assumed 90-degree angle spacer ( $\theta$ ) [49]. Finally, to calculate  $k$  the Sherwood number is calculated [49]:

$$Sh = 0.664k_{dc}Re^{0.5}Sc^{0.33}\left(\frac{2d_h}{l_m}\right)^{0.5} \quad (17)$$

utilizing the Schmidt number:

$$Sc = \frac{\mu}{\rho D} \quad (18)$$

the Reynolds number:

$$Re = \frac{u_x d_h \rho}{\mu} \quad (19)$$

and  $k_{dc}$ , which is defined as the Sherwood spacer correction factor:

$$k_{dc} = 1.654 (d_f/h)^{-0.039} \epsilon^{0.75} (\sin \theta/2)^{0.086} \quad (20)$$

To calculate the Reynolds number, the cross-flow velocity on the exit of the module ( $u$ ):

$$u_x = \frac{Q_c}{wh_{sp}\epsilon} \quad (21)$$

is very important and is affected by the width of the channel ( $w$ ):

$$w = \frac{A_m}{L} \quad (22)$$

where length of the channel ( $L$ ) is defined by the membrane. Density ( $\rho$ ) and viscosity ( $\mu$ ) were assumed at a temperature of 20 °C.

To validate the model, experiments were conducted utilizing one to four membrane modules connected in series. MU-S was circulated at concentrate flow rates of 2.7-3 LPM under constant pressure of 20.7 bar (300 psi). Each experiment was conducted for 15 minutes to avoid permanent scaling to the membranes. Pressure was closely monitored for any increases that could be caused by scaling. Samples from the feed, concentrate, and permeate were collected and SiO<sub>2</sub> concentrations were measured using the Hach methods. After the experiments, a rejection experiment was conducted with a 2,000 mg/L NaCl feed solution to test the integrity of each membrane.

### 2.2.1.7 NF90 scaling experiments

Experiments were conducted to evaluate the scaling tendency of the concentrate from the NF and to investigate a possible pretreatment to protect the integrity of the NF membrane utilizing UF. Scaling of the membrane was tested using an eight times concentrated solution of the MU-S (8x MU-S). 8x MU-S was

selected to accelerate colloidal formation by achieving a concentration higher than 700 mg/L SiO<sub>2</sub>, or the point of zero induction time for colloidal silica formation [19]. The water flux utilizing 8x MU-S water was compared to the water flux of permeate obtained from the UF also utilizing the 8x MU-S as feed (8x MU-S<sub>UFF</sub>). Experiments were conducted at the bench-scale using NF90 flat sheet membranes (0.0139 m<sup>2</sup>). Feed batches of 5 L were recirculated through the system at 1 LPM under constant pressure (10.3 bar (150 psi)) and a constant temperature of 20±1 °C.

## 2.2.2 Membrane distillation

The second option for increasing water recovery using the NF concentrate was MD. Experiments were performed using the 8x MU-S and the UF permeate of the 8x MU-S and 6x MU-S (MU-S<sub>UFF</sub>) as the feed streams and deionized water as the distillate stream.

### 2.2.2.1 Membranes and spacers

Three hydrophobic, microporous membranes were selected for MD testing in this study based on a previous performance study, which compared average water flux, % salt rejection, and thermal efficiency [51]. These include membranes from CLARCOR (QL822; Franklin, TN), 3M (0.2 micron; Maplewood, MN), and Aquastill (0.3 micron; Sittard, The Netherlands). CLARCOR is an asymmetric membrane, made from polytetrafluoroethylene (ePTFE) with a polypropylene support material. It has a thickness of 127-203 μm. An active thickness of 50 μm is assumed in this study. 3M and Aquastill are both isotropic membranes, each with a porosity of 85%. 3M is made from polypropylene and the Aquastill membrane is made from polyethylene.

DelStar Technologies Inc. (Austin, TX) diamond mesh spacers (Product number 113796-0) with 2 mm thickness, were used on each side of the membranes in both the feed and distillate channels of all flow cells. The spacers are made of polypropylene with a filament diameter of 0.9 mm, a mesh size of 4.23 mm, and a hydrodynamic angle of 60°.

Table 2-2. Characteristics of membrane distillation membranes provided by the manufacturers.

Manufacturer	Material	Nominal Pore Size (μm)	Porosity (%)	Thickness (μm)
CLARCOR	ePTFE	0.45	70-85	127-203
3M	polypropylene	0.59	85	110
Aquastill	polyethylene	0.3	85	75

### 2.2.2.2 Test apparatus

Bench-scale tests were performed to determine water flux and scaling tendencies of the MD membranes in an automated, closed loop system. Experiments were conducted using a custom-made acrylic DCMD flow cell with a channel length of 25.4 cm long, 7.62 cm wide, and 0.24 cm thick. The active membrane area was determined by multiplying the channel length by the channel width for a total of 194 cm<sup>2</sup>. Four resistance thermal detectors (Model EI1034, LabJack Corporation, Lakewood, CO) were fitted

to the flow cell to measure and record the temperature at the inlet and outlet of the test cell for both the feed and distillate streams.

Data acquisition and systems control were performed using LabView (National Instruments, Austin, TX) software on a Windows PC and a DAQ device (Model U6, LabJack Corporation, Lakewood, CO). A schematic of the experimental system setup is illustrated in Figure 2-3. The feed solution was pumped continuously using a centrifugal pump and the distillate stream using a positive-displacement gear pump (Micropump, IDEX Corp. Vancouver, WA). The MD system provided heating and cooling to the feed and distillate streams, respectively, using two heat exchangers. Distillate temperature was maintained by adjusting the flow rate of building process chilled water using a proportional valve. The feed solution temperature was maintained using a 1500 W electric immersion heater (Model 1019, Hotwatt, Danvers, MA) that operated based on a target temperature. A PID algorithm, with temperature set points for the feed and distillate streams at the inlet of the module, controlled the operation of the heater and the proportional valve for the distillate cooling.

Conductivity of both the feed and distillate streams were monitored and recorded. Conductivity of the feed was measured at the inlet of the module using a toroidal sensor (Model TCSMA, Sensorex, Garden Grove, CA) and a dip style conductivity probe (Model T-35820-62, Cole-Parmer, Vernon Hills, IL) was installed in the return of the distillate stream. Conductivity was used to calculate the salt rejection of the membrane.

A 10 L PVC tank was fitted with a pressure transducer (PX309 series, OMEGA Engineering, Stamford, CT), at the bottom of the tank to measure the height of water in the tank and thus the volume. Changes in distillate volume were used by the SCADA system to calculate water flux. The distillate tank was also fitted with a solenoid valve to return the distillate to the feed tank periodically during the experiment.

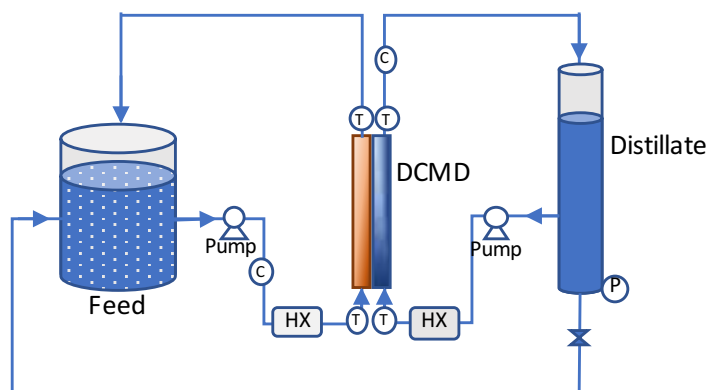


Figure 2-3. MD bench-scale test apparatus. Feed and distillate streams are circulated counter-currently at 1.5 LPM on each side of the membrane. The feed stream is maintained at 60 °C and the distillate stream at 30 °C. A bypass line intermittently returns the distillate to the feed tank to provide a constant feed concentration. T- temperature sensor, C- conductivity sensor, P- pressure transducer, and HX- heat exchanger.

### **2.2.2.3 Experimental procedures**

Experiments were performed to optimize water recovery and investigate scaling tendencies. For each set of experiments a new membrane and new spacer was cut from dry flat sheets and installed into the flow cell. The feed and distillate streams were pumped through the system counter-currently at a constant flow rate of 1.5 LPM. Temperature of the feed solution was maintained at 60 °C and the distillate stream was 30 °C. Between experiments a pH 12 NaOH solution was circulated for several hours to dissolve any residual silica colloids trapped in the system.

Baseline experiments were performed using 3 liters of the 8x MU-S as the feed solution and deionized water as the distillate stream to investigate the scaling tendencies of the NF concentrate from the geothermal make-up water on the membranes. The distillate tank drained 0.5 L to the feed tank after 0.5 L of distillate was produced. Cleaning of the membranes was attempted with a pH 12 NaOH solution [29, 52]. A succeeding experiment was performed under the same operating conditions, utilizing the 3M membrane and a 1 micron cartridge filter (Model 1669T21, McMaster-Carr Supply Company, Elmhurst, IL), installed in the feed line. A third set of experiments, also under the same operating conditions, was conducted without the cartridge filter and utilizing the 8x MU-S<sub>UFP</sub> as the feed stream.

To investigate a sustainable recovery of the MD, a final set of experiments under similar conditions were performed utilizing the 3M membrane and batches of the 8x MU-S<sub>UFP</sub> as the feed stream in an open loop configuration. Four batches of increasing volume (5 L to 8 L) were each concentrated to 1 L or until membrane scaling was observed.

### **2.2.3 Ultrafiltration**

UF had two uses in the study: pretreatment of the NF concentrate to increase water recovery utilizing MD and/or the NF90 and to investigate the maximum mass of colloidal silica that can be recovered by the UF membranes using concentrate from the NF spiral wound experiments as the UF feed (Section 3.2.4 (6x MU-S)).

#### **2.2.3.1 UF membranes**

For this study, a capillary hollow fiber UF membrane acquired from Koch Membrane Systems (Wilmington, MA) was tested in outside-in flow configuration. The outside diameter of the polyvinylidene fluoride (PVDF) fiber membranes used is 2.6 mm, and the nominal membrane pore diameter is 30 nm. Although previous studies have successfully removed colloidal silica utilizing UF membranes with 100 nm pore size, they also have high maintenance costs due to frequent cleanings [34]. The mechanical strength and chemical resistance of PVDF [53] makes it a suitable material for managing tough scalants such as colloidal silica and calcium sulfate that require harsh chemical cleaning.

### 2.2.3.2 Test apparatus

Bench-scale tests were performed to determine critical water flux, permeability, silica rejection, and scaling tendency of the UF membranes as concentrations of colloidal silica increased. Membrane modules were custom-made in the laboratory [54] using 1.27 cm clear PVC pipe as a pressure vessel, and were stored in deionized water at 5 °C until testing. Module 1 was made with five 30.5-cm long fibers glued into the pressure vessel, resulting in a membrane area of 125 cm<sup>2</sup>. Modules 2 and 3 were made with ten 30.5-cm long fibers, resulting in a membrane area of 250 cm<sup>2</sup>.

The flow schematic of the UF bench-scale is shown in Figure 2-4. A 45 L conical-bottom feed reservoir was connected to a centrifugal pump (Micropump, Inc., Vancouver, WA), which continuously pumped 1 LPM, with a corresponding cross-flow feed velocity of 15 cm/s across the 250 cm<sup>2</sup> module and 12 cm/s across the 125 cm<sup>2</sup> module. The permeate side of the membranes were connected to a peristaltic pump (Cole-Parmer, Court Vernon Hills, IL) that provided negative pressure (vacuum) to maintain constant water flux through the membrane. The peristaltic pump was also used to perform backwashing. The permeate was collected in an 8 L tank positioned on an analytical balance (Denver Instrument, Bohemia, NY). The analytical balance and pumps were connected to a SCADA system (U6, LabJack Corporation, Lakewood CO; and LabVIEW, National Instruments, Austin, TX), similar to the system used in the NF apparatus. Changes in permeate mass were used to calculate water flux by the SCADA system. Feed temperature was maintained at 20±1 °C using an immersed cooling-coil. The temperature was controlled by a flow of processed chilled water within the coil that was adjusted using a proportional valve.

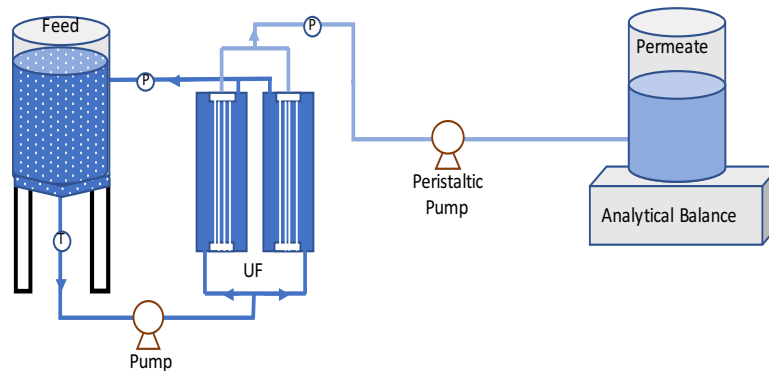


Figure 2-4. Flow schematic of the UF system. Feed was circulated through the modules at a cross-flow velocity of 12-15 cm/s. A peristaltic pump was utilized to provide vacuum pressure and control the flux of permeate. It was also used for backwashing of the membranes. T- temperature sensor, P- pressure transducer.

### 2.2.3.3 Experimental procedures

UF was utilized as pretreatment for MD and NF experiments using NF concentrate water and to recover colloidal silica simultaneously. Experiments were performed to investigate the critical flux and

cleaning techniques for sustainable membrane utilization. UF was also used to evaluate possible recovery of colloidal silica.

#### **2.2.3.4 Permeability tests**

Batch experiments with synthetically reproduced concentrate from the NF (8x MU-S) were performed using the custom-made modules. The first and second batches utilized Module 1 and the third batch utilized Modules 2 and 3 in parallel. Permeability tests were performed to evaluate the integrity of the membranes based on water flux and rejection prior to and post batch testing. Permeability was determined by calculating the slope of the line with water flux as a function of transmembrane pressure (TMP). Average TMP was measured based on 10 minute increments of constant flux ranging from 5 to 25 L/m<sup>2</sup>/h (LMH) in 5 LMH increments. 5 L of a pH 10.5 NaOH solution were utilized in a chemically enhanced backwash (CEB) if the permeability varied by more than 10% from the previous permeability test. The critical flux, defined as “the flux below which a decline of flux with time does not occur; above it fouling is observed” [55, 56], was determined by comparing the deionized water permeability test to a permeability test utilizing 8x MU-S as the feed stream. Results were used to determine the operating flux for the concentration tests. Turbidity rejection tests were performed to investigate the integrity of the membranes utilizing bentonite solution adjusted to 15-20 NTU. Membranes were replaced if the turbidity of the permeate stream was higher than 1 NTU.

#### **2.2.3.5 Concentration experiments**

Concentration experiments were conducted at the critical flux of ~10 LMH with a feed cross-flow velocity of 15 cm/sec. 10.5 L of 8x MU-S as feed was utilized for the first two feed batches. Each batch was treated until ~90% water recovery was achieved. Backwashing with UF permeate was performed for 36 seconds at 80 LMH for both batches; however, backwash trigger mechanisms were different for the two experiments. During the first experiment the backwash was triggered every thirty minutes until 90% water recovery was achieved (30-minute BW). For the second experiment, TMP triggered a backwash at every increase of 0.007 bar, progressing from 0.007 bar to 0.07 bar (0.1-1 psi) (TMP BW). Backwashing flux was determined using the recommended limits provided by the manufacturer.

A 144 L batch of 6x MU-S was utilized as feed in a third experiment to increase the water recovery through the UF membranes and concentrate the colloidal silica to the highest possible percent weight [34]. Feed solution was circulated at 2 LPM through Modules 2 and 3 connected in parallel, resulting in 15 cm/s cross flow velocity in each membrane module. No automatic backwashing was implemented; instead, multiple CEBs were performed during the experiment to maintain membrane permeability. 20 mL samples of the feed solution and permeate were taken at the beginning of all experiments, and at 50, 75, 90, and 95% water recovery. Due to the rapid polymerization rates of soluble silica at a pH of 7, 1 mL of each sample was diluted in 9 mL of deionized water at pH 1. The remaining 19 mL of each sample were preserved at a pH of 12 for 24 hours to dissolve any colloidal silica back to soluble silica.

## CHAPTER 3 RESULTS AND DISCUSSION

Membrane processes were evaluated based on their ability to achieve high water recovery, avoid silica scaling, and recover minerals. Water flux and rejection of ions were measured and used to determine the performance of each membrane process.

### 3.1 OLI stream analyzer simulations

OLI simulations determined the dominant scaling tendencies of the T-MU water based on water recovery with 100% rejection, and temperature. Simulations predicted high scaling tendency for both  $\text{SiO}_2$  and  $\text{CaCO}_3$ , as demonstrated in Figure 3-1. Scaling tendency increased with water recovery for both scalants; however,  $\text{SiO}_2$  was more sensitive to temperature and water recovery than  $\text{CaCO}_3$ . Substantial  $\text{CaCO}_3$  scaling begins around 85% water recovery with an increase in scaling as temperature increases.  $\text{SiO}_2$  scaling begins around 30% water recovery with an increase in scaling as temperature decreases. At 70 °C the tendency of  $\text{SiO}_2$  to scale reaches 1 around 85% recovery, while at 20 °C the scaling tendency of  $\text{SiO}_2$  reaches 1 around 40% water recovery. Significant  $\text{CaCO}_3$  scaling will not occur until a water recovery higher than 90% of the MU-T is achieved, at which point  $\text{SiO}_2$  scaling is already high. Mitigating  $\text{SiO}_2$  scaling will be critical for achieving sustainable processes.

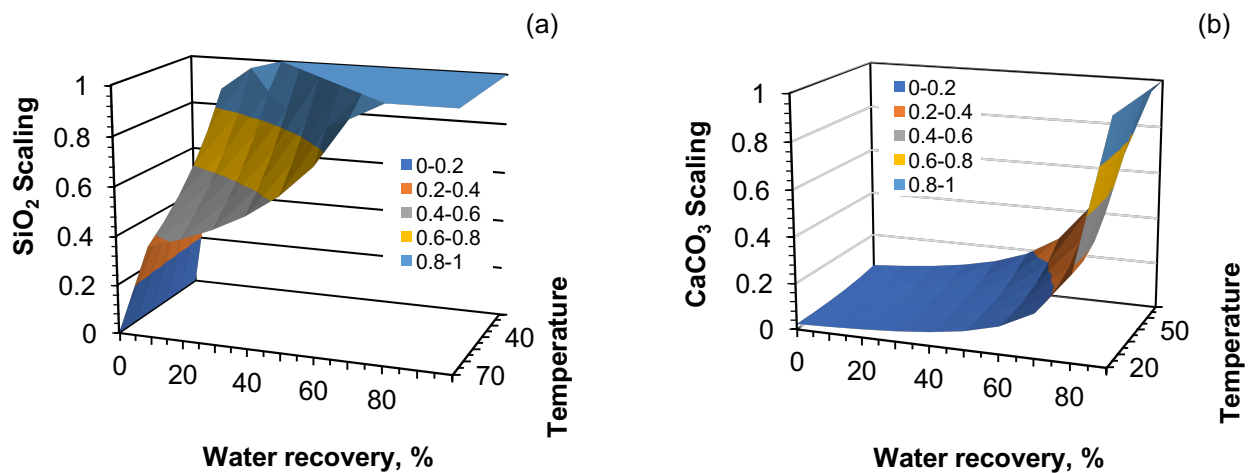


Figure 3-1. OLI prediction of dominant scaling tendencies for (a)  $\text{SiO}_2$  and (b)  $\text{CaCO}_3$ , of T-MU based on water recovery (0 to 90%) and temperature (10 to 70 °C).

### 3.2 Nanofiltration

NF experiments were evaluated based on high water recovery and the membrane's ability to reject silica and other ions present in the MU-T water. NF experiments were also conducted using the NF

concentrate to investigate scaling and a pretreated NF concentrate as a possible option to further increase water recovery.

### 3.2.1 Membrane selection tests

The water flux, percent silica rejection, and percent salt rejection of three waters, MU-T at 20 °C, BI-T at 70 °C, and 2,000 mg/L NaCl at 20 °C (NaCl), were compared at the bench-scale for three NF and one RO membrane as shown in Figure 3-2. Experiments were conducted under constant pressure of 10.3 bar (150 psi) for MU-T and BI-T to match the pressures of the streams at the geothermal power plant. Experiments utilizing NaCl solution were conducted at the same pressure as the rejection experiments (20.7 bar (300 psi)).

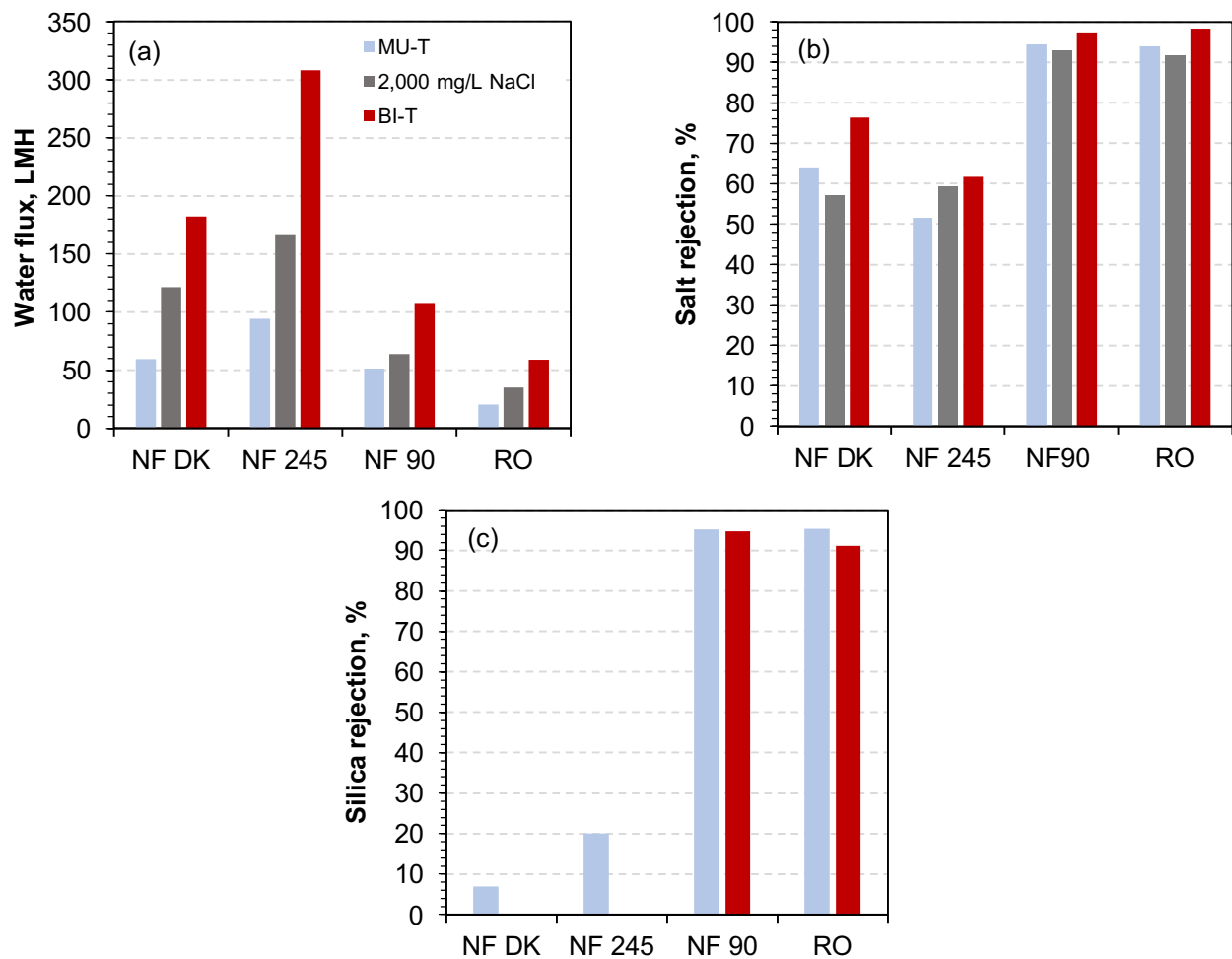


Figure 3-2. (a) Water flux, (b) % salt rejection, and (c) % silica rejection (c) were compared for three NF and one RO membranes (NF DK, NF 245, NF90, and RO SE). 5-hour experiments were performed using flat sheet modules (0.0139 m<sup>2</sup>) for three feed waters: MU-T at 20 °C, 2,000 mg/L NaCl at 20 °C, and BI-T at 70 °C. Feed batches were circulated through the test cell at 1 LPM. Experiments were conducted at constant pressure of 10.3 bar (150 psi) for the MU-T and BI-T waters and 20.7 bar (300 psi) for the NaCl feed waters.

The NF 245 membrane exhibited the highest water flux during testing of the three streams: 308 LMH (BI-T), 94 LMH (MU-T), and 167 LMH NaCl). The RO membrane exhibited the lowest water flux: 59 LMH (BI-T), 20 LMH (MU-T), and 35 LMH (NaCl). The NF90 and NF DK membranes exhibited similar water flux for the MU-T water: 52 LMH and 60 LMH, respectively. However, The NF 245 and NF DK membranes demonstrated the lowest silica and salt rejections, under 20% and 76%, respectively, during testing of the three solutions. The NF90 and RO membranes demonstrated similar salt and silica rejections, with both exhibiting more than 90% rejection during testing with the three solutions. Because silica is a target constituent, the NF DK and NF 245 membranes were omitted from the study. The water flux through the NF90 membrane was more than double the water flux through the RO membrane; therefore, the NF90 membrane was selected for further testing.

### **3.2.2 Synthetic water experiments**

As seen in Table 2-1, the only ions that differ substantially between the water collected on-site (MU-T) and the synthetically reproduced water (MU-S) are sodium and chloride. This is a consequence of balancing ions to match the concentrations of other constituents and pH adjustment using NaOH and HCl. Therefore, experiments were conducted to compare the performance of the NF membrane using the MU-T and MU-S. Results from bench-scale experiments comparing the water flux and rejection of the NF90 at various operating pressures for the synthetic water (MU-S) and the water collected on-site (MU-T) are presented in Figures 3-3. The water flux for the MU-S ranged from 6 LMH at 3.4 bar to 48 LMH at 20.7 bar, while the water flux for the MU-T ranged from 6 LMH to 41 LMH at the same pressures. The membrane demonstrated >95% rejection of all ions in both waters, except for sulfate ( $\text{SO}_4^{2-}$ ) in the MU-T water (77%) and iron (Fe) in the MU-S water (87%). Although the membrane exhibited slightly higher water flux during testing of MU-S water, the difference in flux remained under 20% at all pressures. Difference in rejection of all ions was less than 5%, except for  $\text{SO}_4^{2-}$  rejection, which exhibited 20% higher rejection during testing with the MU-S water. This could be a possible effect of metabisulfite dosing for dechlorinating the deionized water. No scaling tendency was demonstrated for sulfate complexes. Aluminum and iron were measured in trace amounts in the initial analysis of the field sample; however, were not detected in the feed samples during experiments. A third analysis of the field sample also verified that aluminum and iron were not present in the feed water.

Results demonstrated that there was no significant difference between the synthetically reproduced MU-S and the MU-T field sample, suggesting that further testing could proceed utilizing synthetically matched MU-S instead of continuing to collect field samples.

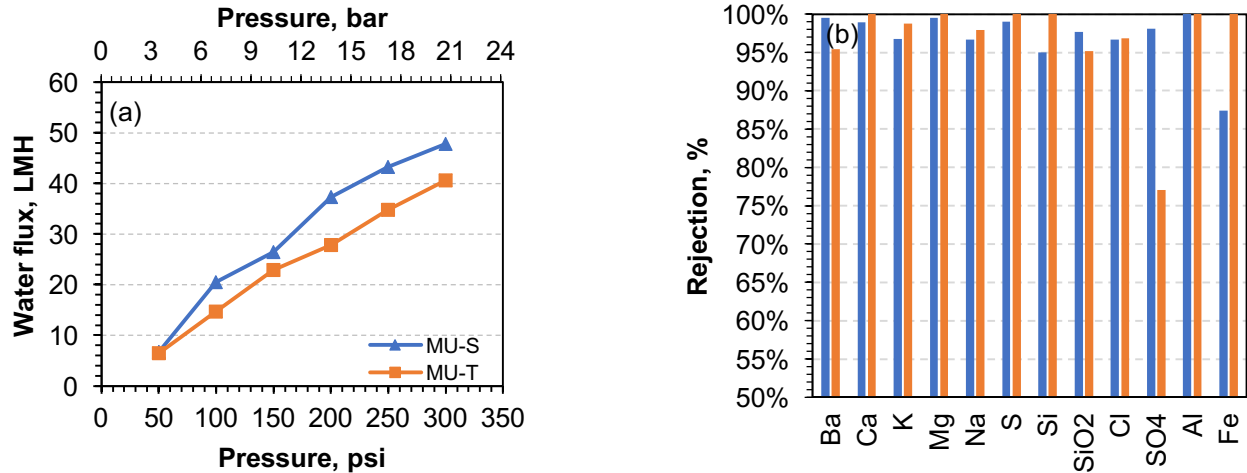


Figure 3-3. (a) Water flux as a function of feed pressure and (b) percent ion rejection during experiments comparing MU-S to the MU-T water. Experiments were conducted with the NF90 membrane. Water was circulated at 1 LPM and was kept at 20±1 °C. Data for ion rejection is from experiments conducted at 10.3 bar (150 psi).

### 3.2.3 Optimization of operating conditions

NF experiments were performed with spiral wound modules in an open loop configuration to validate model predictions of the bulk silica concentrations remaining in the feed and determine operating conditions to achieve the highest water recovery without compromising the integrity of the membranes. Water recovery and concentrations of silica in the feed, permeate, and concentrate were measured at different operating conditions (2.7-3 LPM with one to four NF90-2540 modules connected in series) and compared to the predicted values as shown in Figure 3-4. The concentration of silica in the bulk concentrate stream for 44% water recovery was predicted to be 143 mg/L and measured to be 120 mg/L. At 80% recovery, the maximum water recovery achieved utilizing four NF90-2540 membranes connected in series, the predicted concentration was 403 mg/L and the measured concentration was 435 mg/L. Under these operating conditions, the SiO<sub>2</sub> concentration at the membrane surface is predicted to be 508 mg/L. Rejection tests after 80% water recovery at 20.7 bar (300 psi) showed no decline in water flux through the four membranes (Figure A1 in the appendix). The predicted SiO<sub>2</sub> concentration on the membrane at 80% water recovery was substantially lower than the 600 mg/L limit on the membrane surface because the recovery was limited by the minimum recommended concentrate flow rate of 2.65 LPM for the NF90-2540 membrane module.

Higher water recovery can be achieved without compromising the membranes at lower concentrate flow rates if more membrane modules are operated in series. Results in Figure 3-4b show the concentrate flow needed and corresponding percent water recovery that can be achieved based on the number of modules utilized in series, without exceeding maximum SiO<sub>2</sub> concentration of 600 mg/L on the membrane surface. The recommended minimum concentrate flow of the module is 2.65 LPM; therefore, assuming a water flux of 50 LMH across the NF membrane, 6 modules will be needed to achieve 84% water recovery.

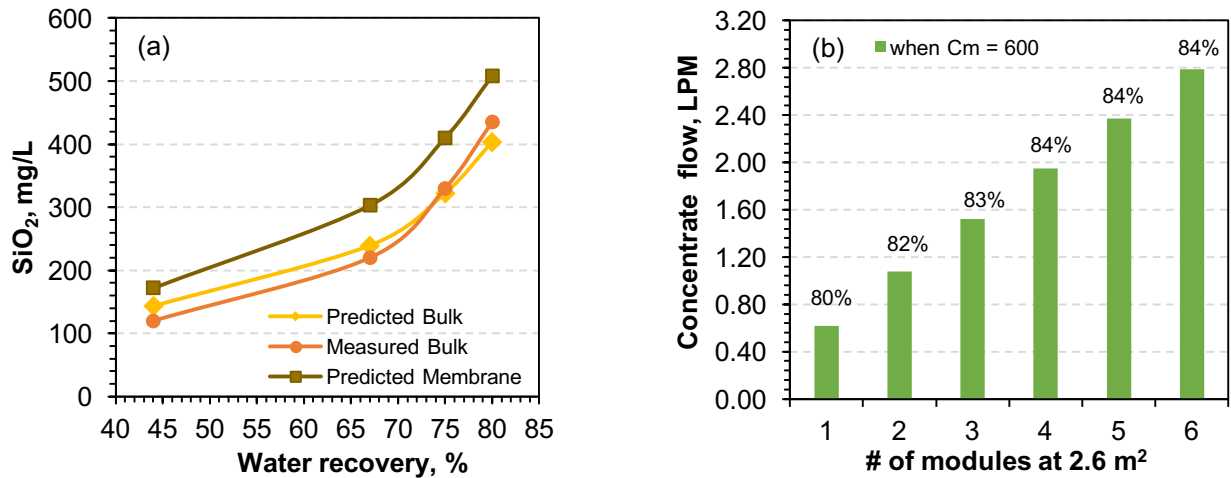


Figure 3-4. (a) Measured concentrations (circle) of silica as a function of % water recovery compared to modeled concentrations in the bulk (diamond) and at the membrane surface (square) as predicted by equations 1 to 21; and (b) predicted concentrate flow and corresponding % water recovery assuming a water flux of 50 LMH as a function of the number of membrane modules connected in series and a maximum concentration of 600 mg/L  $\text{SiO}_2$  on the membrane surface. Experiments were conducted utilizing one to four NF90-2540 spiral wound modules ( $2.6\text{-}10.4 \text{ m}^2$ ). MU-S feed was circulated at 3 LPM and constant pressure was maintained at 20.7 bar.

At 84% water recovery utilizing six modules in series, the concentration of silica predicted in the concentrate stream was 512 mg/L. The measured concentration was 530 mg/L. These results indicate that an approximately six times concentrated solution of the MU-S (6x MU-S) can be achieved in the NF concentrate. The concentrate was sent to the UF membrane to demonstrate recovery of silica colloids and to be utilized as pretreatment for increased water recovery of the MU-S using MD.

### 3.2.4 NF90 scaling experiments

The NF90 membrane was tested in the SEPA-CF test cells to evaluate the effects of scaling utilizing 8x MU-S and UF treated 8x MU-S feed waters. UF was utilized as pretreatment to protect the integrity of the NF membrane and its permeate is designated 8x MU-S<sub>UFP</sub>. Water flux as a function of time is shown in Figure 3-5. An 80% decline in flux was observed after 50 hours of operation utilizing the 8x MU-S (25 LMH to 5 LMH). Testing with the 8x MU-S<sub>UFP</sub> resulted in improved performance of the NF membrane. The initial flux was 35 LMH, 10 LMH higher than the 8x MU-S, and a decline in flux to 20 LMH was observed after 100 hours of operation (43% flux decline). This is most likely due to the presence of colloids that were not rejected by the UF (Figure 3-13). Despite improved performance of the NF90 when desalinating UF-treated water, other desalination processes such as MD, which can withstand higher scaling tendencies, might be preferred for increased recovery when treating high concentration and pretreated silica solutions such as the 8x MU-S<sub>UFP</sub> [57].

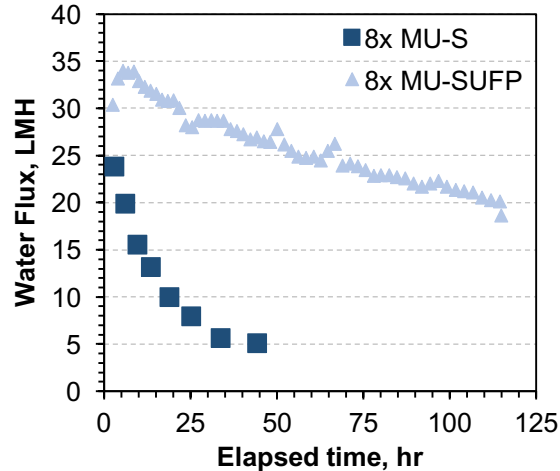


Figure 3-5. Water flux as a function of time for the NF90 flat sheet membranes ( $139 \text{ cm}^2$ ) utilizing the 8x MU-S (squares) and 8x MU-S<sub>UFP</sub> (triangles) as feed waters. Feed water was circulated at 1 LPM and experiments were operated at 10.3 bar.

### 3.3 Membrane distillation

MD experiments were evaluated based on the water flux over time utilizing concentrate from the NF and permeate from the UF. The ability to concentrate the permeate beyond the saturation point of silica was also investigated.

#### 3.3.1 MD scaling experiments

The effects of scaling on the MD membranes was investigated utilizing 8x MU-S and 8x MU-S<sub>UFP</sub>. Membrane scaling experiments were performed using a closed loop cycle with returning of the distillate to the feed every time 0.5 L of distillate crossed the membrane. Water flux as a function of time is illustrated in Figure 3-6. Water flux declined by 80-95% within the first 100-150 hours of the experiment for all three membranes treating/desalinating the 8x MU-S water; however, membrane performance was substantially improved when utilizing the MU-S<sub>UFP</sub> as feed water. Similar to the results of the NF90 (Figure 3-5), the 3M membrane exhibited an initial water flux of 35 LMH, corresponding to 0.75% water recovery, treating both the 8x MU-S and 8x MU-S<sub>UFP</sub>. During operation with the 8x MU-S the flux declined to 5 LMH in less than 20 hours; however, when a cartridge filter was installed in the feed line, only a 5 LMH decline in flux was observed after 80 hours of operation (Figure 3-6a). The experiment was halted after 80 hours due to an increase in pressure observed in the cartridge filter. An attempt to clean the cartridge filter was unsuccessful; therefore, it was not further used in subsequent experiments. A flux decline of 1 LMH was observed after 100 hours of operation with the 8x MU-S<sub>UFP</sub>, demonstrating the ability of MD to withstand higher scaling tendencies compared to the NF, which exhibited a flux decline of 15 LMH under the same conditions (Figure 3-5). The other MD membranes demonstrated similar results to the 3M membrane. The Clarcor membrane exhibited an initial water flux of 30 LMH (0.65% water recovery) utilizing both the 8x MU-S and 8x MU-S<sub>UFP</sub>. The flux declined to 10 LMH after 100 hours of operation utilizing the 8x MU-S; however, almost no flux decline was observed utilizing the 8x MU-S<sub>UFP</sub> (Figure 3-6b). The Aquastill

membrane exhibited an initial flux of 25 LMH (0.54% water recovery) using both feed waters. After 100 hours of operation the Aquastill membrane demonstrated a water flux of 9 LMH treating the 8x MU-S water and 22 LMH treating the 8x MU-S<sub>UFP</sub> water (Figure 3-6c). Although the UF pretreatment substantially improved the performance of the Aquastill membrane, a 12% flux decline was observed. The flux decline is most likely due to the difference in membrane material and morphology. The Aquastill membrane is made out of polyethylene, while the 3M membrane is made out of polypropylene (PP) and the Clarcor membrane is made out of ePTFE. The 3M membrane had the highest initial water flux but it also had the most substantial decline in flux utilizing the 8x MU-S. This is most likely caused by increased concentration and temperature polarization occurring on the membrane surface due to the high flux [47]. However, the decline was mitigated when utilizing the 8x MU-S<sub>UFP</sub>. Therefore, the 3M membrane was selected for further testing.

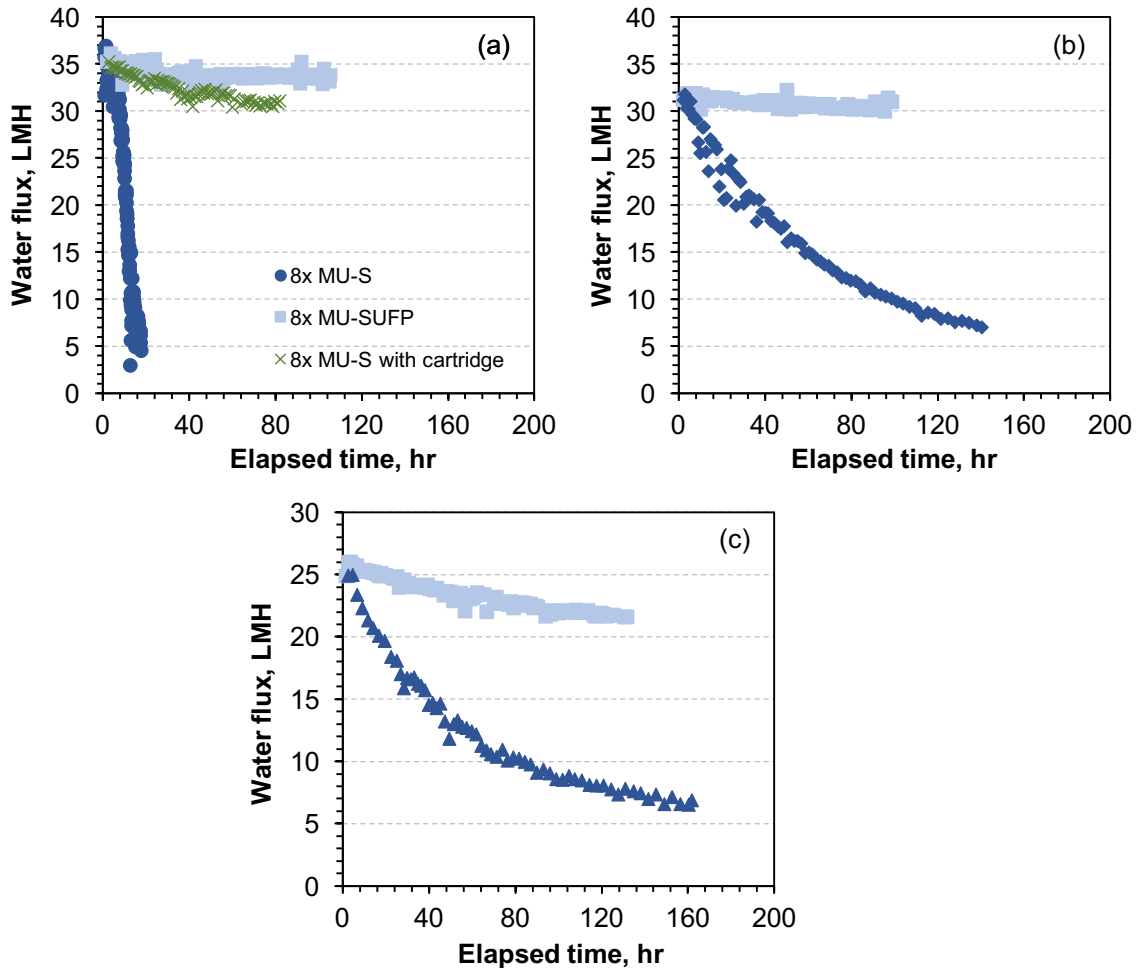


Figure 3-6. Water flux as a function of time utilizing (a) 3M PP 0.2 µm (b) Clarcor QL822 (c) Aquastill 0.3 micron membranes. Feed and distillate streams were circulated through the MD modules (194 cm<sup>2</sup>) at 1.5 LPM utilizing 8x MU-S and 8x MU-S<sub>UFP</sub> at 30/60 °C. An additional experiment with the 3M membrane and 8x MU-S was performed utilizing a cartridge filter in the feed line.

### 3.3.2 MD concentration experiments

Attempting to increase water recovery and approach a ZLD operation, the concentrate from the NF experiments was pretreated through the UF and the permeate was used as feed for the MD process. The experiment was performed under the same operating conditions above, utilizing the 3M membrane and 6x MU-S<sub>UFP</sub> as feed. Distillate was not returned to the feed tank, concentrating the silica by 5-7 times. A sustainable water recovery of MD where scaling does not occur was investigated by increasing the recovery for each batch utilizing the same membrane. The results are illustrated in Figure 3-7. The water flux remained constant for the first three batches (81-87% recovery); however, water flux decline occurred during the fourth batch before 80% recovery was achieved, indicating that 87% water recovery was not sustainable. More experiments need to be performed to evaluate the optimal water recovery for sustainable treatment.

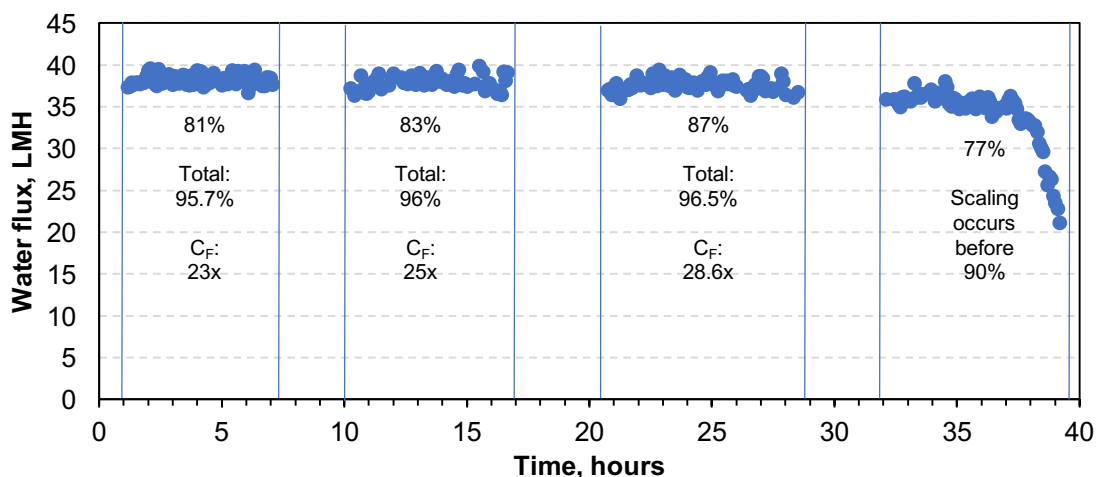


Figure 3-7. Experiments were performed utilizing one 3M membrane and 6x MU-S<sub>UFP</sub> as the feed stream. Four batches of increasing volume (5-8 L) were circulated through the module (0.0194 m<sup>2</sup>) at 1.5 LPM and a temperature difference of 30/60 °C.

After the experiments were performed the concentrate from each batch was collected for future use. Silica concentrations in the concentrate were measured at the end of each experiment. The samples were raised to pH 12 to dissolve silica colloids for measuring soluble SiO<sub>2</sub> using the HACH methods listed previously. When NaOH was added to the samples a floc was observed and the measured concentrations of silica were substantially lower than predicted concentrations (utilizing equations 1 and 2) as shown in Figure A4 in the appendix. Four samples of the concentrate were adjusted to pH 9-12 and compared to the initial sample (measured at pH 8) as shown in Figure 3-8a. As pH increases the floc becomes less dense as demonstrated by the increase in the size of the floc. The floc is most likely the result of silica aggregated to calcium and magnesium that occurs above pH 9 [58]. IC and ICP analysis was performed on the supernatant and the floc to confirm this hypothesis. The results are illustrated in Figure 3-8b. Concentrations of most ions were the same for both the supernatant and the floc except for

silica, calcium and magnesium, which were substantially higher in the floc; therefore, confirming that aggregation was occurring.

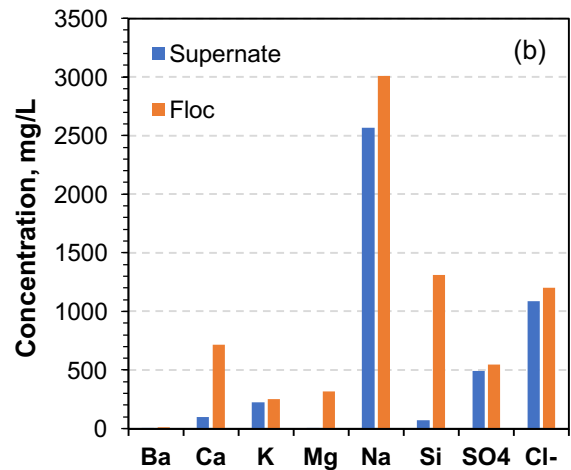


Figure 3-8. MD concentrate of 8x MU-S<sub>UFP</sub> at pH 8 and adjusted to pH 9-12 (left) (b) Concentrations of ions in the supernatant and the floc of the MD concentrate 8x MU-S<sub>UFP</sub> after 87% recovery.

After the MD, the concentrate was collected to use as feed in the UF. The goal for the future is to recover colloidal silica from the MD concentrate while also pretreating it for enhancing water recovery utilizing the MD. This initiates a cycle of recovering high quality water utilizing MD and recovering colloidal silica utilizing the UF.

### 3.4 Ultrafiltration

UF was implemented in the treatment scheme as a pretreatment step of the NF concentrate for MD and to recover colloidal silica. Results were analyzed based on the ability of the membrane to recover colloidal silica and maintain a sustainable operation. Cleaning frequency, permeability, and composition of ions in the feed and permeate were evaluated.

#### 3.4.1 Determination of critical water flux

The critical flux of the 8x MU-S water was determined by comparing the permeability of the membrane utilizing deionized water to the permeability of the 8x MU-S as seen in Figure 3-9a, where the permeability of the membrane is defined as the slope of water flux over TMP (LMH/bar). The point where the permeability of the 8x MU-S water deviated from the pure water was estimated to be around a water flux of 10 LMH. This result is confirmed as illustrated in Figure 3-9b. The TMP at a flux of 10 LMH remains constant while at 15 LMH it substantially increases. Experiments were also performed utilizing higher cross-flow velocity (30 cm/s) (Figure A2 in the Appendix) to increase the critical flux. However, results exhibited no significant differences in critical flux; therefore, experiments were operated at 10 LMH.

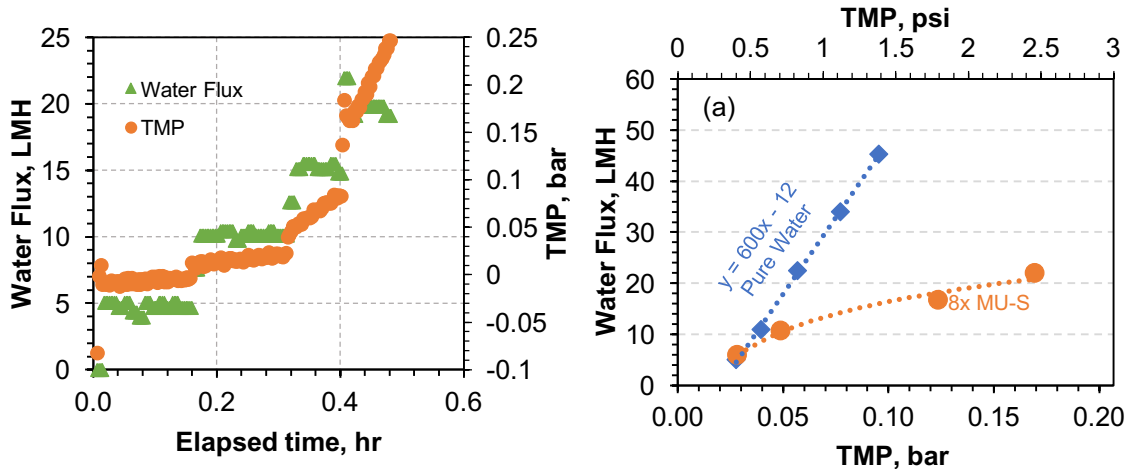


Figure 3-9. (a) Water flux as a function of TMP and (b) water flux and TMP as a function of time. Feed water was circulated at 1 LPM, corresponding to cross flow velocity of 15 cm/s, for 10 minutes at each water flux from 5 to ~50 LMH utilizing a 0.0125 m<sup>2</sup> UF membrane module. Permeability of pure water (diamond) and 8x MU-S (circles) as feed.

### 3.4.2 Optimization of operating conditions

After the critical flux was determined, UF experiments with 10.5 L feed water batch were conducted utilizing a 0.0125 m<sup>2</sup> membrane module to optimize operating conditions for colloidal silica recovery. In the first experiment, automatic backwashing of the permeate was performed for 36 seconds at 80 LMH every 30 minutes as demonstrated in the fluctuations of TMP seen in Figure 3-10a. In the second experiment automatic backwashing (also for 36 seconds at 80 LMH) was triggered by TMP after every increase of 0.007 bar starting at 0.007 (0.1 psi) bar and progressing to 0.07 bar (1 psi). Backwash is demonstrated by the drop in the TMP. After 90% water recovery the TMP increased by 0.03 bar (0.4 psi) during the first experiment and by 0.06 bar (0.9 psi) during the second experiment. Pure water permeability of the membrane was measured at the start and end of each experiment and after CEB with NaOH (Figure 3-7b and d). In the first experiment the initial permeability of pure water was 611 LMH/bar, and it declined to 102 LMH/bar after 90% recovery. After CEB with 5 L NaOH solution at pH 10.5 the pure water permeability was recovered to 489 LMH/bar. In the second experiment the same membrane module was utilized with an initial pure water permeability of 489 MH/bar. After 90% water recovery was achieved, the pure water permeability decreased to 188 LMH/bar and was recovered to 379 LMH/bar after CEB (Figure 3-7c). Results from both experiments revealed that the TMP quickly increased to its original value after backwashing occurred signifying that the backwash did not have a substantial impact on maintaining the permeability of the membrane. This was also seen in the permeability tests performed at the end of the experiments; during the first experiment more frequent backwashing were triggered, resulting in lower water efficiency and therefore a longer operation time to achieve 90% water recovery (>10 hours) and a larger decrease in permeability (611 to 102 LMH/bar vs. 489 to 188 LMH/bar) compared to the second experiment. Based on these results it was concluded that automatic backwashing did not have a substantial impact on membrane performance and was not implemented for

future experiments. However, the CEB was able to recover the permeability from 102 LMH/bar to 489 LMH/bar after the first experiment and from 188 LMH/bar to 379 LMH/bar after the second experiment. These results indicate that operation is potentially sustainable for colloidal silica recovery when utilizing CEB.

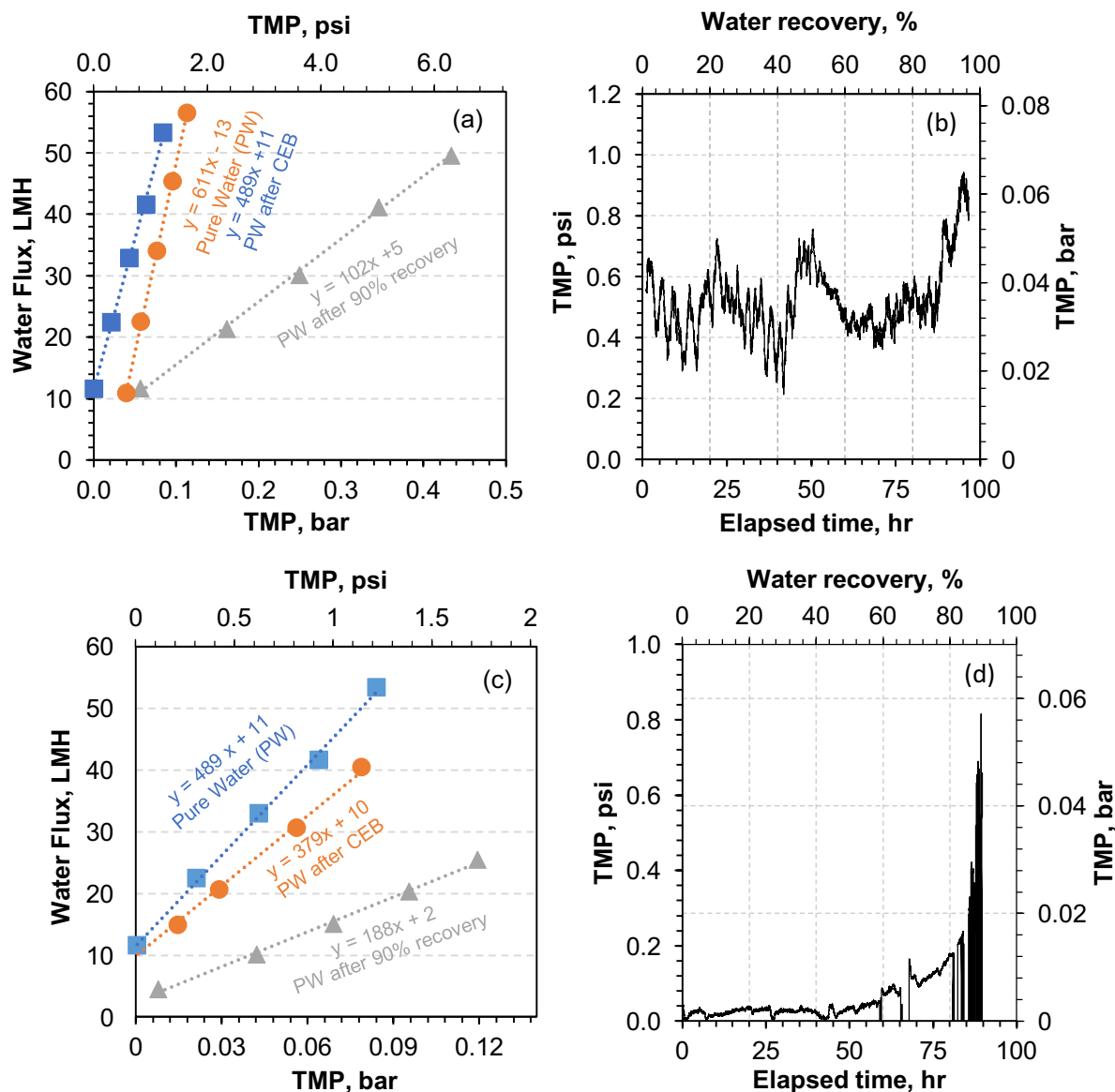
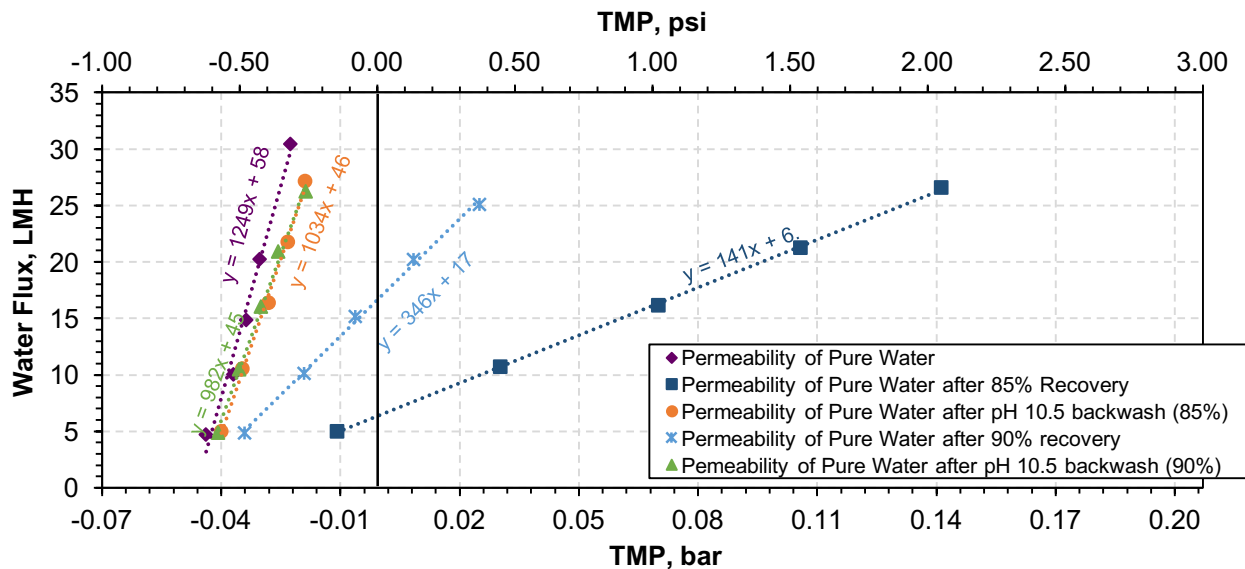


Figure 3-10. (a) permeability tests performed before the experiment, after 90% recovery, and after CEB during the first test, (b) TMP as a function of time up to 90% water recovery with automatic backwashing every 30 minutes as demonstrated by the fluctuations during the first test (c) permeability tests performed before the experiment, after 90% recovery, and after CEB during the second test, and (d) TMP as a function of time up to 90% water recovery with automatic backwashing triggered by an increase in TMP during the second test. Backwash is seen by the drop in TMP to 0. Square symbols: original permeability, round symbols: permeability after pH 10.5 backwash, triangle symbols: permeability after 90% recovery.

### 3.4.3 UF colloidal silica concentration experiments

After potential sustainable membrane operation was demonstrated in the previous experiments, an experiment to recover the highest possible percent by weight of colloidal silica was performed utilizing the concentrate from the NF. 144 liters of 6x MU-S (as predicted by NF spiral wound experiments in section 3.2.4) was used as feed and concentrated utilizing two 0.025 m<sup>2</sup> UF membrane modules operated in parallel. The water flux was maintained at 10 LMH with a corresponding cross-flow velocity of 15 cm/s in each membrane. The pure water permeability of the membranes was measured separately for each module at the beginning of the experiment, and then before and after CEB. The results for module #2 are shown in Figure 3-8. The initial permeability of the membranes was approximately 1,249 LMH/bar. The first CEB was manually initiated after 85% water recovery (and 250 hours of operation) when the TMP increased from 0.09 bar to 0.16 bar. Results of the TMP as a function of time/water recovery are shown in Figure A-3 in the appendix. Before CEB, the pure water permeability had decreased to about 141 LMH/bar; however, after CEB the permeability was recovered to approximately 1,034 LMH/bar. The TMP decreased back to its initial pressure of 0.09 bar. The second CEB was performed after the TMP increased from 0.09 bar to 0.3 bar, and when 90% water recovery was achieved. The pure water permeability was 346 LMH/bar before CEB and 982 LMH/bar after CEB.



concentration was 4,589 mg/L equating to approximately 0.5% weight of colloidal silica in 15 L of feed water. After the second CEB, to concentrate the colloidal silica was continued past 90% water recovery; however, the TMP started to increase immediately with an increase of 0.07 bar occurring within the first hour (Figure A-3 in the Appendix), indicating that 10 LMH was no longer the critical flux for this concentration. A third CEB was performed and the permeate flux was adjusted to 5 LMH. An additional 7 liters were recovered, increasing the total recovery to 95% and the TMP to 0.29 bar. Subsequently, a fourth CEB was performed and the subsequent pure water permeability of the membrane was 45 LMH/bar, a 48% decrease from the initial pure water permeability of 86 LMH/bar. This result and the frequent CEB that were performed after 90% water recovery indicated that concentration of colloidal silica past 0.5% weight utilizing the UF was not sustainable. One factor limiting the maximum concentration of colloidal silica in the UF was the low cross-flow velocity of 15 cm/s. Although doubling the cross-flow velocity did not affect the critical flux, in a report produced by Lawrence Livermore National Laboratory, cross-flow velocities as high as 335 cm/s (11 ft/sec) were necessary to achieve 20-30% silica by weight [34]. While this show feasibility of higher silica recovery, it comes with a higher energy cost to maintain such high crossflow velocity and its associated pressure.

Another limiting factor was the increase in viscosity of the feed. Between 90% and 95% water recovery large flocs were observed in the feed water as seen in Figure 3-9. The experiment was halted and a feed sample was collected for analysis. The supernatant was decanted from the floc and each solution was tested separately utilizing Hach SiO<sub>2</sub> methods, IC, ICP, and particle analysis.

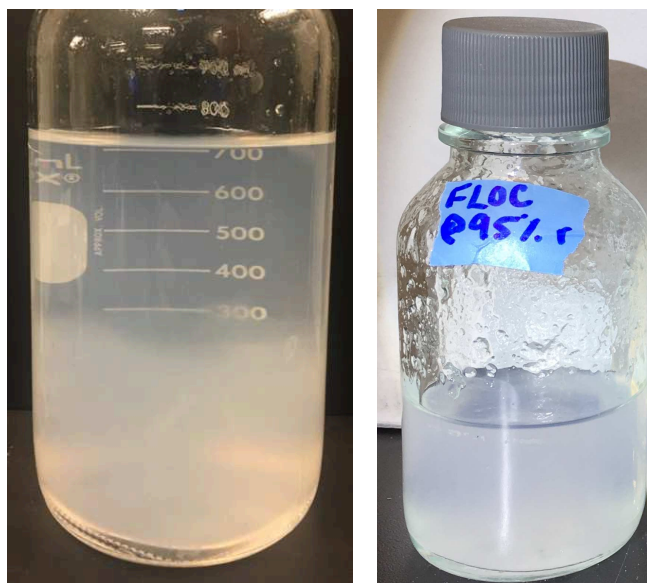


Figure 3-12. Feed water after 95% water recovery before separating floc and supernatant (left) and separated floc (right).

Samples of the UF feed were also drawn at the beginning of the experiment and at 25, 50, 75 and 90% water recovery. Silica concentrations were predicted using Equations 1, 2, and 5 and compared to

measured concentrations utilizing the Hach SiO<sub>2</sub> HR methods (Figure 3-10). The initial concentration of total silica was measured in the feed stream at 530 mg/L and colloidal silica was 420 mg/L. Based on equation 2, the concentration of total silica in the feed after 25%, 50%, 75%, and 90% water recovery was predicted to be 667 mg/L, 938 mg/L, 1,842 mg/L, and 4,165 mg/L, respectively. Measured concentrations were 800 mg/L, 1,000 mg/L, 2,000 mg/L, and 4,000 mg/L. Rejection of silica was maintained by the membranes above 97%, increasing to 99.6% at 90% water recovery; however, at 95% recovery, silica rejection was measured at 93% and accounted for in the predicted concentration of colloidal silica in the feed, resulting in a concentration of 4,721 mg/L. Yet, the measured concentration of colloidal silica was 2,360 mg/L. Rejection tests utilizing bentonite were performed and rejection of the membranes were measured at 99% indicating that the integrity of the membranes was not compromised. A test measuring the rejection of colloidal silica at a lower concentration also demonstrated 98% rejection, indicating that another mechanism was affecting the decrease in rejection of silica at the high concentrations.

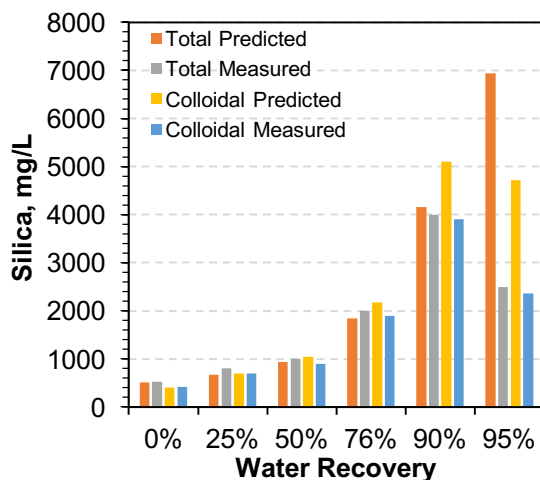


Figure 3-13. Total and colloidal silica concentrations as a function of water recovery. Concentrations were compared to the predicted values utilizing mass balance and equations 1, 2, and 5 and the initial measured feed concentrations of total and colloidal silica.

Measured values closely matched the predicted values of total and colloidal silica with an increase in concentration at each water recovery up to 90%. However, between 90% and 95% water recovery a substantial amount of total and colloidal silica was lost. Predicted concentrations account for the decrease of rejection that was also observed at 95% water recovery. Therefore, the loss of silica concentration was most likely due to the deposition of gel seen on the membranes, the floc formed in the feed solution, and increased frequency of backwashing events. These results are both indicators of different mechanisms of colloidal formation as affected by pH and other salts present in the water. When colloidal silica at pH 8 is in solution at a high salt content for longer than one day, a viscous gel is formed [40]. Further analysis of the gel utilizing SEM and EDS, was conducted to confirm this hypothesis.

CEB loosened the gel and it was physically recovered from the UF modules. The product was freeze-dried and analyzed using SEM and EDS as illustrated in Figure 3-11. SEM results revealed that the

product recovered from the membrane was solid block shape about 1 mm in size at 100x magnification. A smooth surface was observed on the outside, which is explained by the migration of fine particles to the outside surface due to drying mechanisms [59]. Broken pieces of gel exposed a rough surface with high porosity, which is characteristic of colloidal silica gel [59]. The maximum obtainable magnification of this instrument was 10,000x (10  $\mu\text{m}$  scale); however, this corresponds with a significant decrease in the resolution and results were discarded. EDS results also confirmed that substantial silica weight was accumulated in the gel because oxygen and silica were the dominant constituents, making up 97.5% of the solids on the membrane. The remaining gel was retrieved from the membrane, dried overnight, and weighed at 3.33 grams. However, this value was included in the mass balance predicting a total silica concentration of 6,940 mg/L, which was still substantially higher than the measured total silica concentration of 2,500 mg/L. Therefore, the ion composition and concentration of the floc was necessary to establish the amount of silica that was lost due to frequent cleaning compared to the true concentration recovered in the floc.

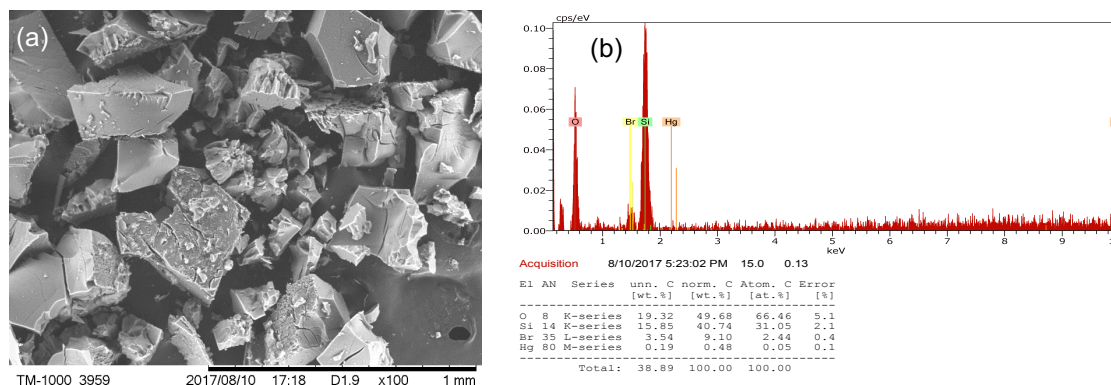


Figure 3-14. (a) SEM micrograph at 100x magnification and (b) EDS chromatograph of a silica gel recovered from the UF membrane modules after 95% recovery. The gel was freeze dried for 24 hours before analysis.

The floc was unable to be re-dissolved into deionized water and was observed sticking to the sides of sample vials, therefore multiple analyses were conducted to determine the composition including IC and ICP and particle size analysis. 40 mL samples were also collected at 75% water recovery for particle size and composition analysis. Particle size results are shown in Figure 3-12a and indicated that there was no difference in size between the supernatant after 95% water recovery and the feed after 75% water recovery, both having an average particle size of 0.18  $\mu\text{m}$  and a standard deviation of 0.04  $\mu\text{m}$  and 0.06  $\mu\text{m}$ , respectively.

The floc after 95% recovery had slightly larger particles, with an average particle size of 0.19  $\mu\text{m}$  and a standard deviation of 0.2  $\mu\text{m}$ . This indicates that a different particle is formed in the floc. This is most likely due to the formation of silica colloids and aggregating with other ions present in the feed such as magnesium and calcium [40, 58]. Particle size analysis was also performed on the initial feed water of the UF (6x MU-S). The average particle size was 0.29  $\mu\text{m}$  with a standard deviation of 0.13  $\mu\text{m}$ . Particles in

the 6x MU-S water obtained from the UF have substantially larger particle size due to the lower concentration of silica. As silica concentration increases nucleation increases with particles beginning to agglomerate above 1000 mg/L [60, 61]. Transmission electron microscopy (TEM) will be required to obtain photomicrographs of particles of this size. IC and ICP results are necessary to determine the purity of the floc.

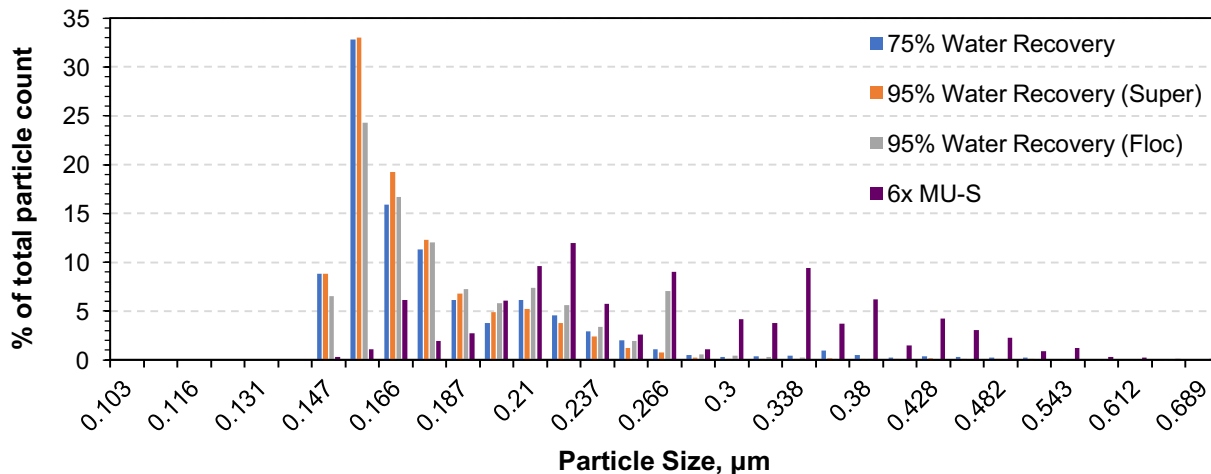


Figure 3-15. particle size analysis of silica in 6x MU-S, after 75% water recovery, and after 95% water recovery (supernatant and floc) for the UF concentration experiments.

The composition of the feed water after 75 and 90% water recovery was compared to the initial composition of the feed. After 95% water recovery a floc was observed in the feed, and concentrations of both the floc and the supernatant were measured. Total silica concentrations increased substantially between the initial feed water and after 75 and 90% water recovery (530 mg/L to 2,180 mg/L and to 4,690 mg/L); however, a substantial decrease in silica concentration was observed after 95% water recovery. Concentrations of the other constituents were maintained in the feed despite concentrating the feed by 4 and 10 times as presented in Table 3-1.

Table 3-1. Water quality of the 8x MU-S UF feed water after 0%, 75%, 90%, and 95% water recovery, measured using IC and ICP methods. 95% water recovery was separated into two samples based on composition: supernatant 95% (S) and floc 95% (F). Concentrations were measured in mg/L.

	Na <sup>+</sup>	K <sup>+</sup>	Mg <sup>2+</sup>	Ca <sup>2+</sup>	Ba <sup>2+</sup>	Cl <sup>-</sup>	SO <sub>4</sub> <sup>2-</sup>	SiO <sub>2</sub>
<b>0%</b>	599	71.5	19.6	76.7	1.76	1,379	99.2	530
<b>75%</b>	582	72.4	17.0	72.0	1.22	1,088	142	2,168
<b>90%</b>	600	71.2	19.5	74.1	1.44	1,227	102	4,689
<b>95% (S)</b>	474	16.0	20.7	79.7	1.02	1,058	99.0	2,981
<b>95% (F)</b>	500	15.4	28.3	99.3	1.79	1,077	94.0	3,413

IC and ICP results of the supernatant and the floc recovered after 95% water recovery showed similar concentrations with slightly higher concentrations of silica, magnesium, and calcium in the floc, indicating that between 90 and 95% water recovery colloidal silica began to aggregate. These results also indicate

that substantial mass of silica and potassium was lost to the frequent cleaning between 90 and 95% recovery.

Relative (%) composition of ions present initially in the feed and after 75 and 90% water recovery, are illustrated in Figure 3-13. Initially, approximately 75% of the feed was made up of other ions with chloride accounting for approximately 45% of total composition; however, as water recovery increased, the relative composition of silica increased from 24% of the total ions to 53% of the total ions after 75% water recovery, and to 70% of the total ions after 90% water recovery. While concentrations of colloidal silica were increasing with recovery, concentrations of other ions were remaining constant. The rejection of all ions by the UF is presented in Figure 3-13b. The rejection of silica was substantially higher (97%) compared to the rejection of the other ions (<15%). Rejection of barium, magnesium, sodium, and sulfate were under 5%, while the rejection of calcium and chloride was under 10%. Therefore, most of the ions were passing through the membrane into the permeate while rejecting the silica to return to the feed. These results indicate that as water recovery increases, the purity of silica colloids also increases.

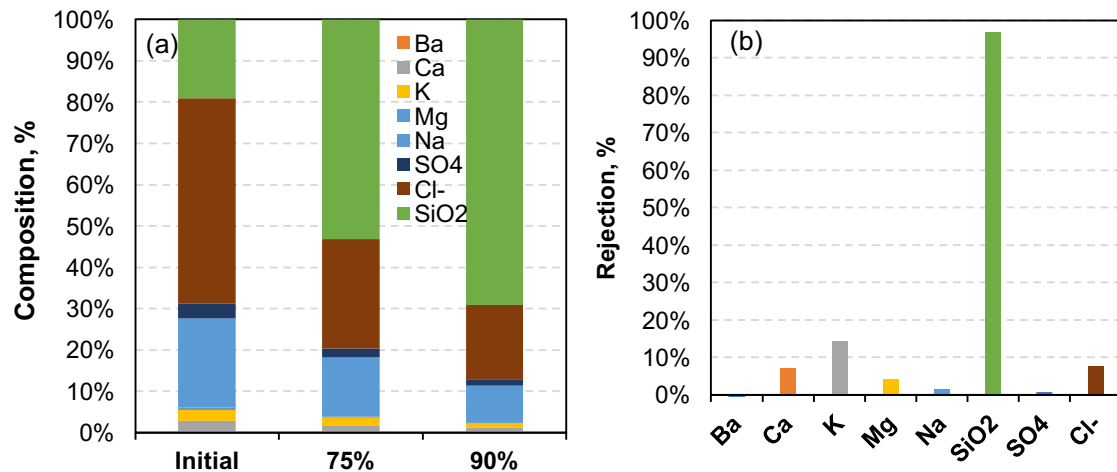


Figure 3-16. (a) % composition of all ions in the UF feed water after 75% and 90% water recovery. (b) UF rejection of all ions in the feed water after 90% water recovery.

## CHAPTER 4

### CONCLUSIONS

A three-system desalination treatment scheme combining NF, UF, and MD was investigated for the treatment of geothermal make-up water containing high silica concentrations. A model to predict the concentration of silica occurring on the membrane surface of the NF was successfully validated utilizing different water recoveries and concentrations of silica in the concentrate. The model predicted optimal operating conditions to maximize water recovery of the NF (83%) while also mitigating hard silica scale due to concentration polarization; therefore, effectively confirming the assumption of sustainable operation. The model would be further strengthened by applying the conditions in future experiments for long-term continuous operation. Future experiments applying higher temperatures to the NF feed could also be utilized to achieve higher water recovery without compromising the integrity of the NF membrane.

Following NF, UF pre-treatment of the NF concentrate for use in the MD was proven to effectively reduce silica scaling at supersaturation concentrations. The UF was also successful in separating colloidal silica from other salts in the geothermal water for extraction. The final products were a silica gel and 0.5% weight colloidal silica, which are both of market value. Market demand for silica gel is growing; however, purifying the silica further utilizing methods such as diafiltration would substantially increase the market value. Future experiments utilizing UF membranes with a smaller pore size could increase the rejection of smaller silica colloids; therefore, increasing the concentration to 1% weight and subsequently increase the value. This could also allow for direct recycling of the UF permeate to the NF. Substantially increasing the cross-flow velocity will increase the sustainable concentration factor. Applying CEB of the UF effectively maintained the integrity of the membranes up to 90% water recovery, therefore proving sustainable operation with colloidal silica.

The final process in the treatment scheme was MD. As mentioned above, the UF pretreatment of the NF concentrate substantially improved the performance of the MD membrane therefore proving an effective increase in the total water recovery of the three-system design. Future experiments continuously recycling the MD concentrate into the UF and the UF permeate into the MD could eliminate a liquid discharge and result in higher amounts of colloidal silica for extraction. Further experiments are also necessary to determine a sustainable recovery of the MD. However, if 65-80% water recovery on the MD is proven for long term operation, coupling it with 83% water recovery from the NF and 90% water recovery from the UF, the three-systems will demonstrate a total water recovery of 93-95%. This is substantially higher than the 63% that is currently achieved in the cooling tower. These results demonstrate that with pretreatment and mineral recovery, silica scaling can be mitigated and high-quality water can be obtained in a sustainable process for use in the geothermal cooling towers. Cost analysis, including energy offsets from utilizing the low-grade geothermal heat and cost offsets from the recovered silica will determine the viability of this three-tier treatment scheme on a larger scale.

## REFERENCES CITED

- [1] A. Bennett, "Developments in desalination and water reuse," *Filtration + Separation*, vol. 52, pp. 28-33, 2015/07/01/ 2015.
- [2] J. G. Herman, C. E. Scruggs, and B. M. Thomson, "The costs of direct and indirect potable water reuse in a medium-sized arid inland community," *Journal of Water Process Engineering*, vol. 19, pp. 239-247, 2017/10/01/ 2017.
- [3] J. J. Klemeš, "Industrial water recycle/reuse," *Current Opinion in Chemical Engineering*, vol. 1, pp. 238-245, 2012/08/01/ 2012.
- [4] Q. K. Tran, D. Jassby, and K. A. Schwabe, "The implications of drought and water conservation on the reuse of municipal wastewater: Recognizing impacts and identifying mitigation possibilities," *Water Research*, vol. 124, pp. 472-481, 2017/11/01/ 2017.
- [5] N. Ghaffour, T. M. Missimer, and G. L. Amy, "Technical review and evaluation of the economics of water desalination: Current and future challenges for better water supply sustainability," *Desalination*, vol. 309, pp. 197-207, 2013/01/15/ 2013.
- [6] J. Imbrogno and G. Belfort, "Membrane Desalination: Where Are We, and What Can We Learn from Fundamentals?," *Annual Review of Chemical and Biomolecular Engineering*, vol. 7, pp. 29-64, 2016.
- [7] M. W. Shahzad, M. Burhan, L. Ang, and K. C. Ng, "Energy-water-environment nexus underpinning future desalination sustainability," *Desalination*, vol. 413, pp. 52-64, 2017/07/01/ 2017.
- [8] A. Ali, R. A. Tufa, F. Macedonio, E. Curcio, and E. Drioli, "Membrane technology in renewable-energy-driven desalination," *Renewable and Sustainable Energy Reviews*, vol. 81, pp. 1-21, 2018/01/01/ 2018.
- [9] M. Lee, A. A. Keller, P.-C. Chiang, W. Den, H. Wang, C.-H. Hou, *et al.*, "Water-energy nexus for urban water systems: A comparative review on energy intensity and environmental impacts in relation to global water risks," *Applied Energy*, vol. 205, pp. 589-601, 2017/11/01/ 2017.
- [10] A. Al-Karaghoul and L. L. Kazmerski, "Energy consumption and water production cost of conventional and renewable-energy-powered desalination processes," *Renewable and Sustainable Energy Reviews*, vol. 24, pp. 343-356, 2013/08/01/ 2013.
- [11] T. J. Feeley, T. J. Skone, G. J. Stiegel, A. McNemar, M. Nemeth, B. Schimmoller, *et al.*, "Water: A critical resource in the thermoelectric power industry," *Energy*, vol. 33, pp. 1-11, 2008/01/01/ 2008.
- [12] V. G. Gude, "Geothermal source potential for water desalination – Current status and future perspective," *Renewable and Sustainable Energy Reviews*, vol. 57, pp. 1038-1065, 2016/05/01/ 2016.
- [13] R. Y. Ning, A. J. Tarquin, and J. E. Balliew, "Seawater RO treatment of RO concentrate to extreme silica concentrations," *Desalination and Water Treatment*, vol. 22, pp. 286-291, 2010/10/01 2010.

- [14] S. Salvador Cob, C. a Beupin, B. Hofs, M. M a Nederlof, D. Harmsen, E. Cornelissen, *et al.*, *Silica and silicate precipitation as limiting factors in high-recovery reverse osmosis operations* vol. 423-424, 2012.
- [15] R. Semiat, I. Sutzkover, and D. Hasson, *Scaling of RO membranes from silica supersaturated solutions\*\** vol. 157, 2003.
- [16] H.-P. Boehm, "The Chemistry of Silica. Solubility, Polymerization, Colloid and Surface Properties, and Biochemistry. Von R. K. Iler. John Wiley and Sons, Chichester 1979. XXIV, 886 S., geb. £ 39.50," *Angewandte Chemie*, vol. 92, pp. 328-328, 1980.
- [17] N. A. Milne, T. O'Reilly, P. Sancio, E. Ostarcevic, M. Beighton, K. Taylor, *et al.*, "Chemistry of silica scale mitigation for RO desalination with particular reference to remote operations," *Water Res*, vol. 65, pp. 107-33, Nov 15 2014.
- [18] K. W. Lawson and D. R. Lloyd, "Membrane distillation," *Journal of Membrane Science*, vol. 124, pp. 1-25, 1997/02/05/ 1997.
- [19] H. P. Rothbaum and A. G. Rohde, "Kinetics of silica polymerization and deposition from dilute solutions between 5 and 180°C," *Journal of Colloid and Interface Science*, vol. 71, pp. 533-559, 1979/10/01/ 1979.
- [20] V. Gekas and B. Hallström, "Mass transfer in the membrane concentration polarization layer under turbulent cross flow: I. Critical literature review and adaptation of existing sherwood correlations to membrane operations," *Journal of Membrane Science*, vol. 30, pp. 153-170, 1987/02/01/ 1987.
- [21] R. Sheikholeslami, "Assessment of the scaling potential for sparingly soluble salts in RO and NF units," *Desalination*, vol. 167, pp. 247-256, 2004/08/15/ 2004.
- [22] T. Koo, Y. J. Lee, and R. Sheikholeslami, "Silica fouling and cleaning of reverse osmosis membranes," *Desalination*, vol. 139, pp. 43-56, 2001/09/20/ 2001.
- [23] M. J. M. White, J.L. Jr.; Gare, S.G., "reverse osmosis pretreatment of high silica waters," SUEZ2017.
- [24] L. Song, J. Hu, S.-L. Ong, J. Ng, M. Elimelech, and M. Wilf, *Performance limitation of the full-scale reverse osmosis process* vol. 214, 2003.
- [25] M. Paul and S. D. Jons, "Chemistry and fabrication of polymeric nanofiltration membranes: A review," *Polymer*, vol. 103, pp. 417-456, 2016/10/26/ 2016.
- [26] A. M. O. Mohamed, M. Maraqa, and J. Al Handhaly, "Impact of land disposal of reject brine from desalination plants on soil and groundwater," *Desalination*, vol. 182, pp. 411-433, 2005/11/01/ 2005.
- [27] A. Alkudhiri, N. Darwish, and N. Hilal, "Treatment of high salinity solutions: Application of air gap membrane distillation," *Desalination*, vol. 287, pp. 55-60, 2012/02/15/ 2012.
- [28] E. Curcio, X. Ji, A. M. Quazi, S. Barghi, G. Di Profio, E. Fontananova, *et al.*, "Hybrid nanofiltration–membrane crystallization system for the treatment of sulfate wastes," *Journal of Membrane Science*, vol. 360, pp. 493-498, 2010/09/15/ 2010.
- [29] E. Drioli, E. Curcio, A. Criscuoli, and G. D. Profio, "Integrated system for recovery of CaCO<sub>3</sub>, NaCl and MgSO<sub>4</sub>·7H<sub>2</sub>O from nanofiltration retentate," *Journal of Membrane Science*, vol. 239, pp. 27-38, 2004/08/01/ 2004.

- [30] F. He, J. Gilron, and K. K. Sirkar, "High water recovery in direct contact membrane distillation using a series of cascades," *Desalination*, vol. 323, pp. 48-54, 2013/08/15/ 2013.
- [31] F. Macedonio, E. Drioli, E. Curcio, and G. Di Profio, "Experimental and economical evaluation of a membrane crystallizer plant," *Desalination and Water Treatment*, vol. 9, pp. 49-53, 2009/09/01 2009.
- [32] M. Safavi and T. Mohammadi, "High-salinity water desalination using VMD," *Chemical Engineering Journal*, vol. 149, pp. 191-195, 2009/07/01/ 2009.
- [33] Y. Yun, R. Ma, W. Zhang, A. G. Fane, and J. Li, "Direct contact membrane distillation mechanism for high concentration NaCl solutions," *Desalination*, vol. 188, pp. 251-262, 2006/02/05/ 2006.
- [34] W. Bourcier, C. Bruton, S. Roberts, S. Viani, S. Conley, and S. Martin, "Co-Production of Silica from Geothermal Fluids," Livermore, CA2009.
- [35] J. A. Epstein, "Utilization of the dead sea minerals (a review)," *Hydrometallurgy*, vol. 2, pp. 1-10, 1976/07/01/ 1976.
- [36] K. L. Hickenbottom and T. Y. Cath, "Sustainable operation of membrane distillation for enhancement of mineral recovery from hypersaline solutions," *Journal of Membrane Science*, vol. 454, pp. 426-435, 2014/03/15/ 2014.
- [37] D. L. Gallup, "Geochemistry of geothermal fluids and well scales, and potential for mineral recovery," *Ore Geology Reviews*, vol. 12, pp. 225-236, 1998/06/01/ 1998.
- [38] A. Maimoni, "Minerals recovery from salton sea geothermal brines: a literature review and proposed cementation process," *Geothermics*, vol. 11, pp. 239-258, 1982/01/01/ 1982.
- [39] H. H. Werner, "Contribution to the mineral extraction from supersaturated geothermal brines Salton Sea Area, California," *Geothermics*, vol. 2, pp. 1651-1655, 1970/01/01/ 1970.
- [40] R. K. Iler, *The Chemistry of Silica*. New York, 1979.
- [41] T. Oertel, U. Helbig, F. Hutter, H. Kletti, and G. SEXTL, "Influence of amorphous silica on the hydration in ultra-high performance concrete," *Cement and Concrete Research*, vol. 58, pp. 121-130, 2014/04/01/ 2014.
- [42] W. Bourcier, C. Bruton, S. Roberts, S. Viani, S. Conley, and S. Martin, "Pilot-scale geothermal silica recovery at Mammoth Lakes," Lawrence Livermore National Laboratory, Livermore, CA CEC-500-2009-077, 2009.
- [43] M. Cheryan, *Ultrafiltration Handbook*: Technomic Publishing Company, Inc., 1986.
- [44] X. Shi, G. Tal, N. P. Hankins, and V. Gitis, "Fouling and cleaning of ultrafiltration membranes: A review," *Journal of Water Process Engineering*, vol. 1, pp. 121-138, 2014/04/01/ 2014.
- [45] A. D. Eaton, M. A. H. Franson, A. P. H. Association, A. W. W. Association, and W. E. Federation, *Standard Methods for the Examination of Water & Wastewater*: American Public Health Association, 2005.
- [46] "Water Analysis Guide," ed. Loveland, CO: Hach Company, 2013.
- [47] J. A. Bush, J. Vanneste, and T. Y. Cath, "Membrane distillation for concentration of hypersaline brines from the Great Salt Lake: Effects of scaling and fouling on performance, efficiency, and salt rejection," *Separation and Purification Technology*, vol. 170, pp. 78-91, 10/1/ 2016.

- [48] M. Mulder, *Basic Principles of Membrane Technology*. Dordrecht: Kluwer Academic Publishers, 1996.
- [49] A. R. Da Costa, A. G. Fane, and D. E. Wiley, "Spacer characterization and pressure drop modelling in spacer-filled channels for ultrafiltration," *Journal of Membrane Science*, vol. 87, pp. 79-98, 1994/02/23/ 1994.
- [50] K. R. Applin, "The diffusion of dissolved silica in dilute aqueous solution," *Geochimica et Cosmochimica Acta*, vol. 51, pp. 2147-2151, 1987/08/01/ 1987.
- [51] J. Vanneste, J. A. Bush, K. L. Hickenbottom, C. A. Marks, D. Jassby, C. S. Turchi, *et al.*, "Novel thermal efficiency-based model for determination of thermal conductivity of membrane distillation membranes," *Journal of Membrane Science*, 2017.
- [52] J. A. Bush, J. Vanneste, E. M. Gustafson, C. Waechter, and T. Y. Cath, "Prevention and management of silica scaling in membrane distillation using pH adjustment," *Desalination*, 2018.
- [53] G.-d. Kang and Y.-m. Cao, "Application and modification of poly(vinylidene fluoride) (PVDF) membranes – A review," *Journal of Membrane Science*, vol. 463, pp. 145-165, 2014/08/01/ 2014.
- [54] S. M. Riley, Oliveira, J.M.S., Regnery, J., Cath, T.Y., "Hybrid membrane bio-systems for sustainable treatment of oil & gas produced water and frac flowback," *Separation and Purification Technology*, vol. 171, pp. 297-311, 2016.
- [55] R. W. Field, D. Wu, J. A. Howell, and B. B. Gupta, "Critical flux concept for microfiltration fouling," *Journal of Membrane Science*, vol. 100, pp. 259-272, 1995/04/28/ 1995.
- [56] D. Wu, J. A. Howell, and R. W. Field, "Critical flux measurement for model colloids," *Journal of Membrane Science*, vol. 152, pp. 89-98, 1999/01/06/ 1999.
- [57] C. R. Martinetti, A. E. Childress, and T. Y. Cath, "High recovery of concentrated RO brines using forward osmosis and membrane distillation," *Journal of Membrane Science*, vol. 331, pp. 31-39, 2009/04/01/ 2009.
- [58] J. S. Gill, "Inhibition of silica—silicate deposit in industrial waters," *Colloids and Surfaces A: Physicochemical and Engineering Aspects*, vol. 74, pp. 101-106, 1993/07/06/ 1993.
- [59] E. Pecoraro, M. R. Davolos, and M. Jafelicci, "SILICA MORPHOLOGY CHARACTERIZED BY SEM - THE EFFECTS OF THE SOLVENT TREATMENT AND THE DRYING PROCESS," *Journal of the Brazilian Chemical Society*, vol. 6, pp. 337-341, 1995.
- [60] E. D. E. R. Hyde, A. Seyfaee, F. Neville, and R. Moreno-Atanasio, "Colloidal Silica Particle Synthesis and Future Industrial Manufacturing Pathways: A Review," *Industrial & Engineering Chemistry Research*, vol. 55, pp. 8891-8913, 2016/08/24 2016.
- [61] M. Kley, A. Kempter, V. Boyko, and K. Huber, "Mechanistic Studies of Silica Polymerization from Supersaturated Aqueous Solutions by Means of Time-Resolved Light Scattering," *Langmuir*, vol. 30, pp. 12664-12674, 2014/10/28 2014.

APPENDIX A

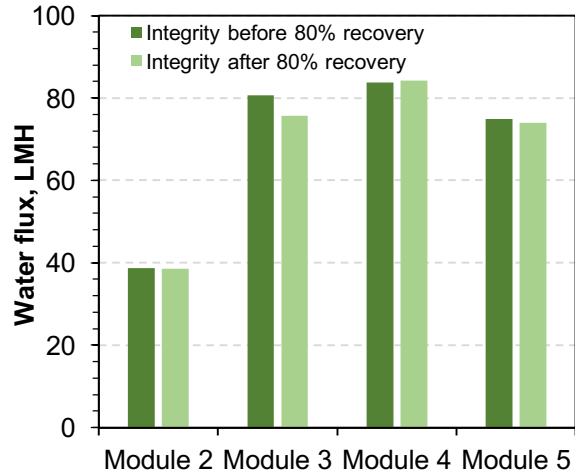


Figure A-1. Integrity of each membrane before and after model validation experiments. Integrity tests were operated at 3 LPM, 20.7 bar and 20 °C utilizing a 2,000 mg/L NaCl solution.

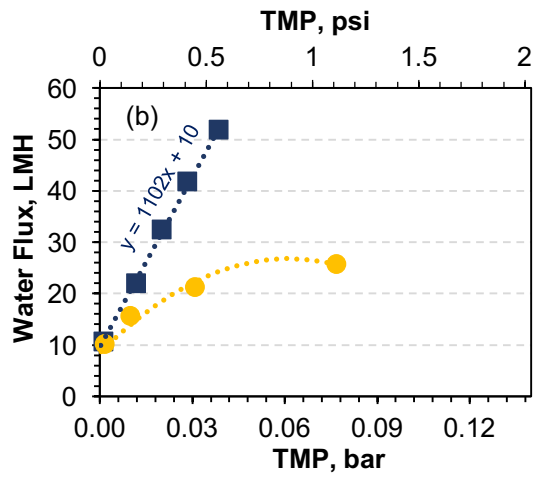


Figure A-2. The permeability of UF membrane (0.025 m<sup>2</sup>) utilizing pure water (squares) and 8x MU-S (circles). Feed water was circulated at 2 LPM, corresponding cross flow velocity of 30 cm/s, for 10 minutes at each water flux from 5-50 LMH.

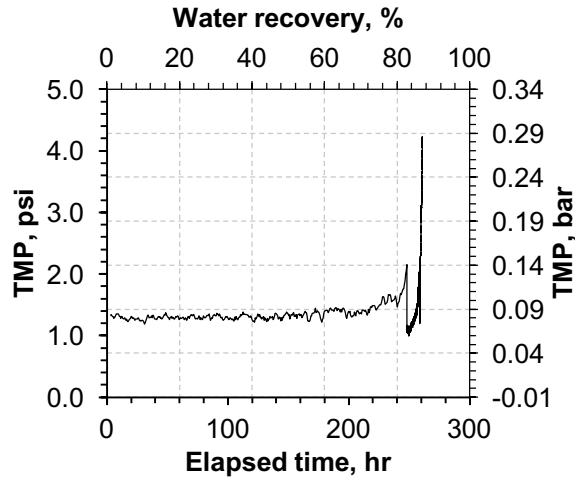


Figure A-3. TMP based on water recovery and time utilizing 144 L of 6x MU-S. The experiment was performed utilizing two ( $0.0250 \text{ m}^2$ ) modules in parallel. Feed was circulated at 2 LPM corresponding to 15 cm/s cross-flow velocity of each module. CEB backwashing was performed after 85% water recovery and after 90% water recovery demonstrated by the drop in TMP.

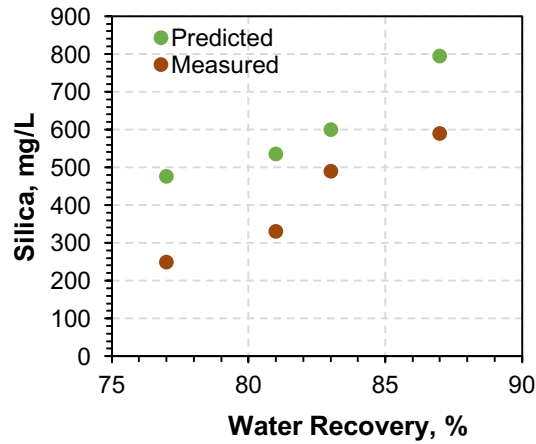


Figure A-4. Measured and predicted concentrations of silica in the MD feed. Experiments were performed utilizing one 3M membrane and 6x MU-S<sub>UFP</sub> as the feed stream. Four batches of increasing volume (5-8 L) were circulated through the module ( $0.0194 \text{ m}^2$ ) at 1.5 LPM and a temperature difference of 30/60 °C.